Approximate Calculation of Conversion with Kinetic Normalization for Finite Reaction Rates in Wall-Coated Microchannels

J. P. Lopes and Alírio E. Rodrigues
Dept. of Chemical Engineering, Laboratory of Separation and Reaction Engineering, Associate Laboratory LSRE/LCM, Faculty of Engineering, University of Porto

Silvana S.S. Cardoso
Dept. of Chemical Engineering and Biotechnology, University of Cambridge, Cambridge, U.K

DOI 10.1002/aic.12483
Published online January 19, 2011 in Wiley Online Library (wileyonlinelibrary.com).

We consider the problem of mass transfer in a channel with wall reaction and present approximate results to describe the conversion profile. We report analytical solutions in both Graetz's and Lévêque's regime in cases where only (semi)numerical studies have been presented before. In particular, for first-order kinetics under conditions of a fully developed concentration profile, an approximate procedure for conversion calculation is proposed for finite reaction rates. When the profile is developing, asymptotic limits are used to formulate accurate approximations in intermediate parametric ranges. Moreover, the effect of finite reaction rates in the corrections due to curvature or velocity profile nonlinearities are reported. Finally, we extend the previous results to an m*th order "power-law" wall reaction, so that kinetic normalization is achieved in suitable limits. These results are of relevance for the modeling and simulation of processes involving catalytic monoliths or microreactors.* © 2011 American Institute of Chemical Engineers *AIChE J,* 57: 2870–2887, 2011
Keywords: mathematical modeling, mass transfer, reactor analysis, monoliths, microreactors

Introduction

The analysis of flow and mass transfer in a channel with reactive surfaces has been considered useful in modeling several chemical engineering related problems: CVD processes,[1] electrochemical systems,[2] and catalytic monoliths[3–5] among others. Recently, the problem has been again an object of great attention in the context of coated-wall microreactors.[6–8] In this case, employing very thin catalytic layers deposited on high thermal conductivity supports allows reduction of mass transfer resistance, good thermal management and lower pressure drops, which has been exploited in a wide range of practical applications, from energy-related to biocatalytic transformations.

The conceptual descriptions of the problems mentioned earlier are very similar and they usually involve coupling between flow and mass transfer in the channel domain, with reaction (and eventual further diffusion) at the catalytic layer. The simplest physical picture is the one where reactant species is transported axially by convection and axial diffusion and, towards the walls of the channel, by transverse diffusion. The resulting conservation equation (without the axial diffusion term) has been solved analytically for convective heat transfer in tubes, with uniform wall temperature or flux conditions. Early independent works include the ones by Graetz,[9] Paneth and Herzfeld,[10] and Nusselt[11] as given credit by Damköhler.[12]

Correspondence concerning this article should be addressed to J. P. Lopes at deq07006@fe.up.pt.

Table 1. Summary of Some Relevant Previous Studies and Contribution of this Work

Approach	References
Graetz solution series	
Numerical calculation of eigenvalues and constants for specified values of *Da* and common cross-section geometries (first order wall reaction)	3,13–17
Asymptotic approximations limited to specific ranges (infinitely fast or slow wall reaction rate)	18–25
Uniformly valid analytical approximation for the first eigenvalue and weight for any value of *Da* with no fitting parameters (first order wall reaction)	This work (Graetz-Nusselt regime section)
Lévêque's solution	
Analytical solution with first order wall reaction and Lévêque's original assumptions (additional numerical evaluation required for laminar flow)	14,26–28
Approximate solution to Lévêque's problem and first-order reaction kinetics with no numerical evaluation involved	This work (Lévêque's regime section)
Extended Lévêque solutions in the Dirichlet and Neumann limits (analogy with heat transfer)	29–32
Corrections to extended Lévêque solutions accounting for finiteness of first order reaction kinetics	This work (Lévêque's regime section)
Reaction kinetics other than first-order	
Numerical	3,33
Zero-order reaction	18,34–36
Integral equation methods	33,37–40
Explicit approximations for power-law kinetics in fully developed and developing concentration profile	This work (Kinetic normalization section)

These well-known solutions for the concentration (or temperature) profile involve an infinite sum of terms, each one with coefficients that usually require numerical evaluation (see Table 1). Moreover, in the case of a first-order reaction occurring at the walls of the channel, the dependence of such coefficients on the wall reaction parameter is complex and an explicit relationship has not been obtained for finite reaction rates.

Another issue is that in some cases (especially for short distances from the inlet or high flowrates) a satisfactory solution demands a large number of terms to be retained in the slowly convergent series. For this reason, the analysis of this problem is divided in two main regimes:[40] Graetz's regime (where concentration changes over the length scale of the channel transverse characteristic dimension) and Lévêque's regime (when such variation occurs in a thin region near the walls of the channel). In particular, when only one term in Graetz's series reasonably describes the solution, the concentration profile is said to be ''fully developed,'' while for developing profile conditions, Lévêque's approach[42] has been extensively used to circumvent the convergence problems associated with the convection-dominated regime. Housiadas et al.[22] compared several approximations to evaluate the terms in Graetz series with uniform wall concentration, including asymptotic expansions using the WKB method[17] and Lévêque-type solutions,[20] stressing the numerical issues in the accurate calculation of these quantities. In the case of finite reaction rates, a number of studies are available (see Table 1), which usually involve numerical evaluation for particular parametric sets. Thus, the effect of kinetics has not been presented explicitly.

In this work, we revisit the problem of convective diffusion inside a wall-coated channel, where an isothermal heterogeneous reaction is occurring. Approximate analytical solutions for the concentration profile inside the channel allow us to obtain accurate estimates for the conversion variation along the channel, with minimal numerical evaluation and explicit parametric dependence. Moreover, asymptotic limits can be identified and help to understand the effects of the following: (a) the relative importance of mass transport mechanisms (namely, the length scale over which transverse diffusion effects are relevant, distinguishing two main regimes), (b) curvature (considering parallel plates and circular channel geometries), (c) flow profile (both plug and laminar flow), (d) kinetics (the condition of finite wall reaction rate as an intermediate between uniform wall flux and concentration boundaries), and (e) reaction rate expression (in particular, the influence of the order of reaction m in a ''power-law'' kinetics type).

We use two strategies: (a) calculation of higher-order terms in a perturbative scheme whenever possible (Lévêque's extended regime and corrections for the m order ''power law'' kinetics in the ''Kinetic normalization'' section); and (b) ''matching'' limits by empirical formulas without introducing too much complexity (approximations to eigenvalues and constants in ''Graetz- Nusselt regime'' section). In the case of a first-order reaction, both approaches are done with the purpose of extending the range of validity of asymptotic expansions and describe successfully the solution in intermediate parametric ranges. Although the application of some of these procedures is known in the limiting cases of very slow or fast reactions (Table 1), when the reaction rate is finite no approximate solutions exist. In fact, most treatments of the problem require numerical evaluation, which may be inconvenient when: (i) parametric studies in broad ranges are to be performed, (ii) large-scale systems (composed e.g., by several microchannels in a parallel configuration) are being considered, or (iii) numerical difficulties occur, arising e.g., from near zero wall concentration and noninteger reaction exponents. Moreover, this will leave the parametric dependence of the systems' performance implicit. Table 1 summarizes previous work as well as the contribution of the present work.

Graetz-Nusselt Regime (Dominant Transverse Diffusion and Convection)

In a microchannel with small aspect ratio, but when the constant times for transverse diffusion and convection are comparable, the classical Graetz-Nusselt problem[10] is recovered in

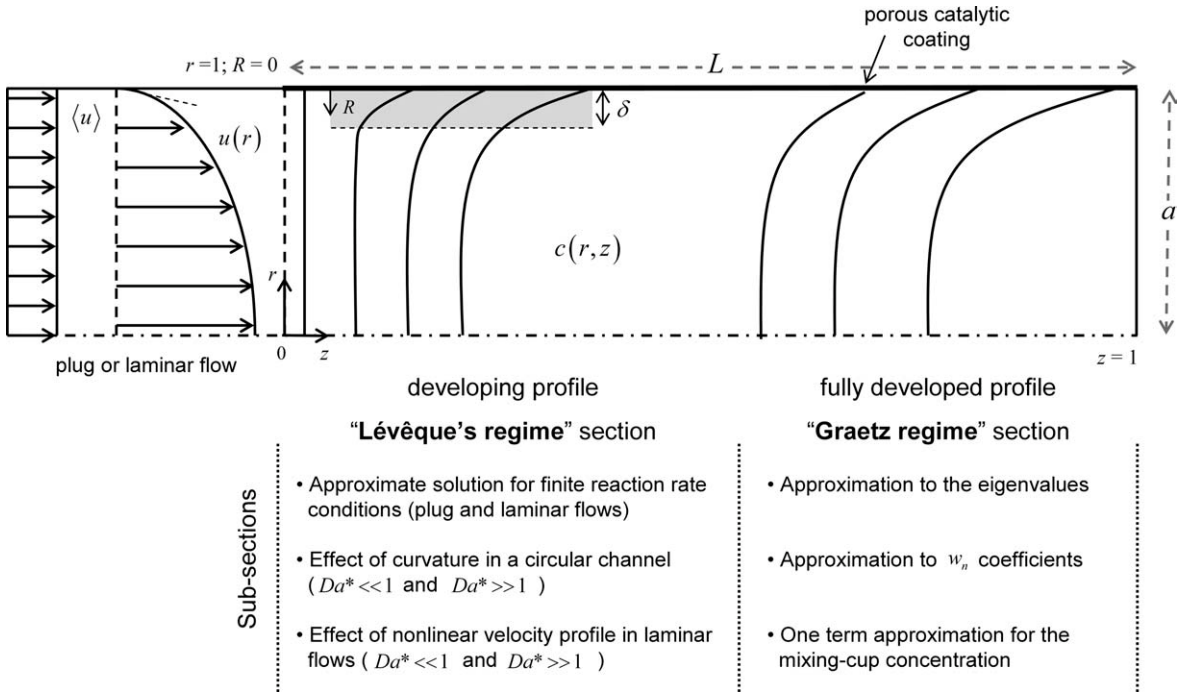

Figure 1. Schematic representation of the concentration profile in the channel domain showing the two main mass transfer regimes considered in this work.

In each case, the detailed analysis in suitable limits can be found in the presented subsections.

the channel domain [where $z \sim O(1)$]. In this section, we start by identifying the main quantities needed for calculating the concentration profile (and conversion) in the channel. Next, we present our approximate expressions that will allow us to estimate conversion as a function of the parameters involved. We then compare our approximate predictions with numerical results from gPROMS®.

Theoretical background

We consider straight parallel plate or circular channels with uniform cross-sectional area, in isothermal steady-state operation, coupled with a first-order heterogeneous reaction in a porous catalytic coating with uniform properties (Figure 1). Under these assumptions, the convective diffusion equation is[42,43]

$$\frac{\partial^2 c}{\partial x^2} = \alpha Pe_m v(x) \frac{\partial c}{\partial z} \qquad \text{for parallel plates, and} \tag{1a}$$

$$\frac{1}{r}\frac{\partial}{\partial r}\left(r\frac{\partial c}{\partial r}\right) = \alpha Pe_m v(r) \frac{\partial c}{\partial z} \qquad \text{for a circular channel} \tag{1b}$$

where the dimensionless independent variables are the axial position scaled by the channel length ($z = \hat{z}/L$) and the transverse position within the open channel (normalized by channel radius ($r = \hat{r}/a$) or half-spacing between plates ($x = \hat{\chi}/a$)). The concentration in this domain is written as a fraction of the inlet concentration ($c = \hat{c}/c_{in}$). The dimensionless uniform and parabolic velocity profiles are

$$v(x) = \frac{u(x)}{\langle u \rangle} = \begin{cases} \frac{j+3}{2}(1-x^2) & \text{laminar flow} \\ 1 & \text{plug-flow} \end{cases} \tag{2}$$

where $j = 0$ for parallel plates and $j = 1$ for circular channel.

In Eqs. 1, two dimensionless parameters arise: the transverse mass Péclet number ($Pe_m = \langle u \rangle a/D$) and the channel aspect ratio ($\alpha = a/L$). Axial diffusion is negligible up to $O(\alpha^2)$, i.e., for small aspect ratio channels. In this case ($\alpha \ll 1$), the inlet Danckwerts' boundary condition is simplified to uniform inlet concentration for $Pe_m \gg \alpha$,

$$c(r, 0) = 1. \tag{3}$$

Despite the fact that the two domains (channel and catalytic layer) are coupled, a frequent approach is averaging the latter by using the effectiveness factor (η) concept. It has been pointed out[3,42,45] that for a first-order reaction, the flux continuity requirement writes as a finite wall resistance (Robin-type) boundary condition, even when internal diffusion inside the porous coating must be considered. It can thus be written as

$$\left.\frac{\partial c}{\partial r}\right|_{r=1} = -Da\, c(1, z), \tag{4}$$

where the rescaled Damköhler number ($Da^* = Da^{II}\, \eta\, \delta_R$), accounting for the concentration boundary layer thickness ($\delta_R \sim 1$ in the Graetz regime) could have been used instead. Here, the Damköhler number compares the surface reaction time-

scale with the transverse diffusion one ($= ak_{surf}/D$). In terms of the observed reaction kinetics, Da writes as $Da^{II}\,\eta$. Uniform wall flux (Neumann) and uniform wall concentration (Dirichlet-type) boundary conditions are obtained for $Da \ll 1$ and $Da \gg 1$, respectively.

The well-known solution[9,12] to this problem has the following separable form:

$$c(r,z) = \sum_{n=1}^{\infty} A_n \varphi_n(r) \exp\left(\frac{-\lambda_n^2}{\alpha Pe_{m,\max}} z\right) \tag{5}$$

where $\varphi_n(r)$ is an eigenfunction in the transverse coordinate (r or x), while the exponential term represents the axial dependence of the concentration profile (being $Pe_{m,\max}$ the transverse Péclet number evaluated at the maximum velocity in the channel). Both transverse and axial contributions are associated with λ_n, the n^{th} eigenvalue (a function of Da, in general), which satisfies Eq. 4. The typical dependence of the first eigenvalue on Da is illustrated in Figure 2 (full lines correspond to numerical calculations). Two asymptotes are of interest, corresponding to low and high values of Da. For the former, the leading-order behavior of the first eigenvalue is

$$\lambda_1^2 \sim \sigma Da + O(Da^2) \qquad \text{as} \quad Da \to 0 \tag{6}$$

where $\sigma = (j+1)\frac{u_{\max}}{\langle u\rangle}$ ($j = 0$ or 1 for parallel plates or circular channel, respectively).

On the other hand, near the Dirichlet limit ($Da \gg 1$), the first eigenvalue does not change significantly with Da. Carslaw et al.[13] and Brown[18] calculated these values as

$$\lambda_{1,\infty}^2 = \begin{cases} \pi^2/4 & \text{parallel plates} \\ 5.783 & \text{circular channel} \end{cases} \quad \text{for plug-flow, and} \tag{7a}$$

$$\lambda_{1,\infty}^2 = \begin{cases} 2.828 & \text{parallel plates} \\ 7.313 & \text{circular channel} \end{cases} \quad \text{for laminar flow.} \tag{7b}$$

Finally, A_n is the n^{th} integration constant, which can be calculated from the orthogonality condition (e.g., Townsend,[46] Bauer[14]). The previous results are needed when calculating the mixing-cup concentration:

$$\langle c\rangle(z) = \frac{\int_A u(r)c(r,z)dA}{\int_A u(r)dA}. \tag{8}$$

This is related to the conversion of reactant along the channel (with respect to the inlet concentration), $X_R = 1 - \langle c\rangle(z)$. Substituting solution (5) into Eq. 8 leads to

$$\langle c\rangle(z) = \sum_{n=1}^{\infty} w_n \exp\left(\frac{-\lambda_n^2}{\alpha Pe_{m,\max}} z\right) \tag{9}$$

where w_n are dependent only on Da for each channel geometry and flow profile, and are called in some references[3] as the normalized Fourier weights, or are presented as a combination of integration constants and eigenfunctions derivatives at the wall.

The lowest value of w_1 appears in the Dirichlet limit ($w_{1,\infty}$) and is given for plug-flow conditions by[23]

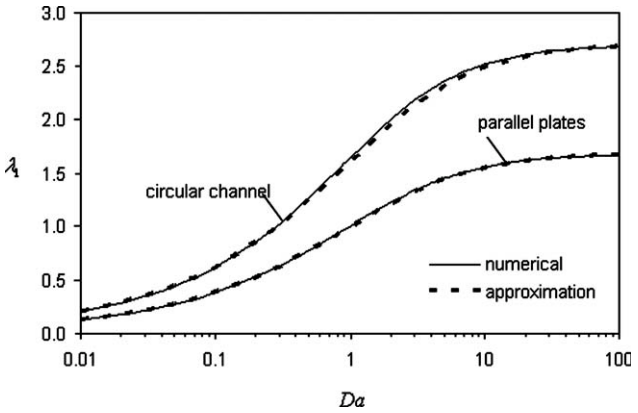

Figure 2. First eigenvalue (λ_1) as a function of the Damköhler number (Da) for laminar flow between parallel plates and inside a circular channel.

Numerical results (full lines) are compared with approximate expression (14) (dashed lines).

$$w_{n,\infty} = 2/\lambda_{n,\infty}^2, \quad \text{parallel plates} \tag{10a}$$

$$w_{n,\infty} = 4/\lambda_{n,\infty}^2, \quad \text{circular channel.} \tag{10b}$$

In the next section, we use WKB results[17] to write $w_{n,\infty}$ for laminar flow.

Frequently,[3,19,47–49] the calculation of $\langle c\rangle(z)$ is simplified by retaining just one term in Eq. 9, leading to

$$\langle c\rangle(z) \sim w_1 \exp\left(\frac{-\lambda_1^2}{\alpha Pe_{m,\max}} z\right). \tag{11}$$

Approximation to the eigenvalues

The calculation of conversion using (11) can be done once approximate dependences for λ_1^2 and w_1 on Da are provided. In this section, we will be concerned with the first eigenvalue.

An improved estimate for λ_1 for large Da is obtained here in an iterative manner, starting with the result in the Dirichlet limit as a first guess, $\lambda_1^{(0)} = \lambda_{1,\infty}$. In this case, an approximation for high eigenvalues but $Da/\lambda_1 \gg 1$ can be useful to characterise how λ_1 approaches $\lambda_{1,\infty}$ in an intermediate range of Da. For plug-flow between parallel plates, Robin's boundary condition can be expanded for large Da/λ_1 as $\lambda_1 = \arctan(Da/\lambda_1) \sim \lambda_1^{(0)} - \lambda_1/Da + \ldots$. Admitting that it is sufficient to retain these terms in the expansion, the improved result writes as

$$\lambda_1 \sim \lambda_{1,\infty}\frac{Da}{1+Da} \tag{12}$$

which, when compared to the numerical solution presents relative error in the range of 10^{-4} –5% for $Da > 1.5$. We apply the same procedure for plug flow in a circular channel, after expanding Bessel functions for large argument. The result is similar to that in Eq. 12 with $\lambda_1^{(0)} \sim 3\pi/4$ and with a relative error of around 2% for $Da > 2$.

For laminar flows, we expand hypergeometric function in $\varphi(x)$ or $\varphi(r)$ for large eigenvalues[51] leading to the following form of Robin's condition:

$$\tan\lambda_1 = \frac{1}{2\lambda_1} + \frac{Da}{\lambda_1} \qquad \text{(for parallel plates)} \tag{13a}$$

$$\tan\left(\lambda_1 - \frac{\pi}{4}\right) = \frac{Da}{\lambda_1} \qquad \text{(for circular channel)} \tag{13b}$$

For large Da/λ_1, the expansion of arctan (x) for large argument in Eqs. 13 leads to a rational function, which can be corrected to the right Dirichlet limit, yielding a relationship like Eq. 12. This result improves the estimate of the eigenvalues for $Da > 1$.

Uniformly Valid Approximation (All Values of Da). The previous results show that: (a) two asymptotic regions exist, where the eigenvalues are well characterized; and (b) the transition from the $Da \sim 1$ region to the Dirichlet limit is well described by a rational function. An approximate expression of the same form of Eq. 12 can be easily conceived using asymptotic methods (e.g., Gottifredi et al.[52]), so that both limits are fulfilled:

$$\lambda_1^2 \sim \frac{Da\ \sigma}{1 + Da\ \sigma/\lambda_{1,\infty}^2} \tag{14}$$

Equation 14 has higher relative error (compared to numerical results) in the range of Da approximately 2–3, which is less than 2.5 or 4% for plug-flow between parallel plates and circular channel, respectively. For laminar flows, the first eigenvalue is predicted with errors just slightly above 1 and 2% for plates and round tube. The numerical results and Eq. 14 predictions are plotted in Figure 2. Expressions for this type have been also sought in other contexts,[52–54] but the final dependence on Da results in much more complicated expressions or are the product of fitting procedures (with numerically evaluated coefficients). Equation 14 gives an extremely simple functional dependence, while retaining the asymptotically correct behavior.

We note that previous literature is full of procedures for calculation of eigenvalues and weights (or related quantities), due to the high importance of estimating conversion (alternatively, mixing-cup temperature) or Sherwood (and Nusselt) numbers. Table 1 provides a short list of some relevant studies concerning the calculation of eigenvalues for Graetz series' terms with first-order wall reaction (more examples could be found in Shah and London[15] or other textbooks). We distinguish between two approaches.

First, and probably more ubiquitous, examples of numerical calculation for only specified values of Da are presented. Secondly, explicit analytical approximations exist but are of extremely limited application, namely high eigenvalues ($n \gg 1$) asymptotics in Dirichlet/Neumann limit, where for example, the effect of finite kinetics on the first (lowest) eigenvalue is ignored (see Table 1).

The asymptotically correct correlation (14) we propose works very reasonably in the intermediate range of $Da \sim 1$. This expression is also attractive when optimal parameter regions are being searched, avoiding extensive numerical evaluation. Moreover, the effects of geometry and flow profile are indicated explicitly.

Approximation to w_n coefficients

Combining Robin's boundary equation with the orthogonality condition, we can obtain a compact result for the integration constant given by

$$A_n = \frac{2Da}{\lambda_n \varphi_n(1)} \left(\frac{dDa}{d\lambda_n}\right)^{-1}. \tag{15}$$

Therefore, when Da is finite ($\sim$1), we use Eq. 15 to obtain

$$w_n \sim \frac{d(\sigma/\lambda_n^2)}{d(1/Da)} \tag{16}$$

The typical dependence of the first Fourier weight (which is also the largest one) on Da is represented by a smooth transition between two asymptotic plateaus in the limits of $Da \to 0$ and $Da \to \infty$. The variation in the intermediate range of Damköhler number is not easily obtained and extending the asymptotic expansions in the limits is beneficial for small and large (finite) Da, but unreasonable when $Da \sim 1$.

When $Da \ll 1$, the first Fourier weight is directly obtained from Eq. 16, once we know that the first eigenvalue in this limit is described by Eq. 6. Thus,

$$w_1(Da \to 0) = 1 - O(Da^2). \tag{17}$$

The Dirichlet limit for plug-flow can be found in Eqs. 10. For fully developed parabolic flow profile, we follow the WKB method[18] to obtain,

$$w_{n,\infty} = \frac{12(3^{5/6})}{\sqrt{\pi}\Gamma(1/6)} \lambda_{n,\infty}^{-7/3} = 3.0384\ \lambda_{n,\infty}^{-7/3} \quad \text{parallel plates} \tag{18a}$$

$$w_{n,\infty} = \frac{32(3^{5/6})}{\sqrt{\pi}\Gamma(1/6)} \lambda_{n,\infty}^{-7/3} = 8.1023\ \lambda_{n,\infty}^{-7/3} \quad \text{circular channel.} \tag{18b}$$

Even though Eqs. 18 were conceived for large eigenvalues (thus, large n), the results for $w_{1,\infty}$ with the appropriate first eigenvalues (Eqs. 7) are in good agreement with numerical solutions for parallel plates ($w_{1,\infty} = 0.9104$) and for circular channel ($w_{1,\infty} = 0.8191$), with maximum relative errors of 1.3% and 0.3%, respectively.

As we saw previously, eigenvalues approach their Dirichlet values $\lambda_{1,\infty}$ according to Eq. 12. This is general for the geometries and flow profiles studied, but more accurate for plug-flow, where the Fourier weight tends to its limit value, $w_{1,\infty}$, as

$$w_1 = \frac{2\sigma}{\lambda_{1,\infty}^2}\left(1 + \frac{1}{Da}\right).$$

We can then say generically that,

$$w_1(Da \to \infty) = w_{1,\infty}\left(1 + \frac{1}{Da}\right) \tag{19}$$

Table 2. Range of *Da* in Which w_1 can be Approximated by Either $w_1 = 1$ ($Da < Da_{max}$) or $w_1 = w_{1,\infty}$ ($Da > Da_{min}$)

			Error <5%		Error <1%	
		$w_{1,\infty}$	Da_{max}	Da_{min}	Da_{max}	Da_{min}
Plug flow	plates	0.8106	2.5	17	0.8	100
	circular	0.6917	2.1	36	0.7	200
Laminar flow	plates	0.9104	5.1	4.1	1.0	34
	circular	0.8191	2.1	12	0.6	70

represents the correct trend in this asymptotic limit. Eq. 19 gives less than 5% relative error in the following ranges: $Da \geq 6$ (plug-flow between parallel plates); $Da \geq 3$ (plug-flow inside a circular channel); $Da \geq 15$ (laminar flow between plates); and $Da \geq 8$ (laminar flow inside circular duct).

Uniformly Valid Approximation (All Values of Da). As expected, the transition from the low-*Da* asymptote ($w_1 \rightarrow 1$) to the high-*Da* asymptote ($w_1 \rightarrow w_{1,\infty}$) in the intermediate region of $Da \sim 1$ is not satisfactorily described by these limits. Table 2 contains the asymptotic values $w_{1,\infty}$ for the geometries and flow profiles studied. Both bounds on w_1($w_1 = 1$ and $w_1 = w_{1,\infty}$) work as approximations outside the intermediate range of *Da*,

$$w_1 \sim \begin{cases} 1, & Da \leq Da_{\max} \\ w_{1,\infty}, & Da \geq Da_{\min} \end{cases}. \tag{20}$$

Values of Da_{min} and Da_{max} are given in Table 2 for maximum relative errors of the first Fourier weight, as given by Eq. 20, of around 5% and 1%. We can see that when $Da \sim 1$, no satisfactory approximation is obtained.

Note that we have more information when *Da* is high: the nonleading order variation is of $O(Da^{-1})$, while the first Fourier weight deviates very slowly ($O(Da^2)$) from 1 as $Da \rightarrow 1$ from 0). Therefore, we construct an uniformly valid approximation from Eq. (19):

$$\frac{w_1 - w_{1,\infty}}{1 - w_{1,\infty}} = \frac{w_{1,\infty}}{(1 - w_{1,\infty})}\frac{1}{Da} \quad \text{as } Da \rightarrow \infty.$$

A simple expression that also allows the small *Da* limit to be fulfilled writes as

$$\frac{w_1 - w_{1,\infty}}{1 - w_{1,\infty}} = \frac{1}{1 + \frac{1 - w_{1,\infty}}{w_{1,\infty}} Da} \tag{21}$$

where $w_{1,\infty}$ is obtained by previously given expressions (independent of *Da*). Of course Eq. (21) is only a particular case of the general empirical equation proposed by Churchill and Usagi[55] to successfully correlate experimental and numerical data for a wide range of problems (e.g., determination of Sherwood and Nusselt numbers as a function of the Damköhler number for triangular channels).[56] Though a wide variety of problems involving functions that approach constant values in both limits have been successfully dealt by this kind of expressions, to the authors' knowledge it so far has not been applied to the prediction of w_1 as a function of *Da* in two-dimensional models.

Eq. (21) can be generalized to a powered addition of asymptotic limits,[55] which results in introducing an extra parameter into the correlation

$$\frac{w_1 - w_{1,\infty}}{1 - w_{1,\infty}} = \left[1 + \left(\frac{1 - w_{1,\infty}}{w_{1,\infty}} Da\right)^b\right]^{-1/b}. \tag{22}$$

The simplest form to determine *b* is to ask for the correlation to produce the correct result when the right-hand side of Eq. (22) is 2, i.e., when $Da = w_{1,\infty}/(1-w_{1,\infty})$. In that case, $b \approx 1$ for plug flow between parallel plates and for laminar flow (circular and slit ducts), but $b \approx 4$ when plug-flow in a circular channel is being studied. However, the numerical results are still well approximated by (22) when *b* changes around these values.

The correlation given by Eq. (21) predicts numerical results for parallel plates with 2.5% maximum error for plug-flow (at $Da \sim 2$), and 2% error for laminar flow (around $Da \sim 8$). For plug-flow inside a circular channel, Eq. (22) with $b \approx 4$ gives less than 6% relative error near $Da \sim 7$ (and about 10% had we considered $b \approx 1$). For laminar flow inside a round tube, only 1.4% maximum error is observed near $Da \sim 1$.

One-term approximation for the mixing-cup concentration

The prediction of the exit mixing-cup concentration from Eq. (11) (with w_1 from Eq. (22) and the first eigenvalue from Eq. (14)) is compared with numerical solution of Eqs. (1) in Figure 3, where the quality of our approximations for the quantities involved in Eq. (11) is tested. We also plot the results in a parametric range where the one-term approximation is expected to fail (large $\alpha\ Pe_m$). The range of $\alpha\ Pe_m < (\alpha\ Pe_m)^*$ where Eq. (11) is applicable is identified for the first time for several representative values of *Da*, as are the magnitudes of error involved.

For $\alpha\ Pe_m \sim O(1)$, the error associated with the approximation is in the range of error involved in the estimation of eigenvalues and Fourier weights. When $\alpha\ Pe_m$ increases, retaining just one term in Eq. (9) is not sufficient (the convection-dominated regime in "Lévêque's regime" section will be appropriate for this limit). This is particularly noticeable at high *Da*, for example, in the case of plug-flow between parallel plates, where error increases from 4 to 11% at $\alpha\ Pe_m = 100$, when *Da* changes from 1 to 10^4. Moreover, in the same situation, less than 5% relative error (in the range of meaningful absolute values for concentration) is obtained only for $\alpha\ Pe_m < 20$ when $Da = 10$ or $Da = 10^4$. The external mass transfer controlled limit is, therefore, the one where convection-dominated solutions are more relevant, due to the existence of a concentration boundary layer.

The same remark can be made when plug-flow in a circular tube is considered. The maximum relative errors occur at high $\alpha\ Pe_m$ and *Da* (around 18% for $Da = 10$ and 10^4, but only 0.2% when $Da = 1$, at $\alpha\ Pe_m = 100$). Maximum of 5% relative error is obtained for $\alpha\ Pe_m < 10$ when $Da = 10$ or 10^4.

For laminar flows (Figure 3 for the case of a round tube), the same observations hold in the high *Da* region: error increases significantly with $\alpha\ Pe_m$ and curvature (maximum errors of 6% in parallel plates and 12% in circular channel, for $\alpha\ Pe_m = 100$ and $Da = 10^4$). The range over which is possible to apply the one-term approximation also gets narrower for circular channel (less than 5% error obtained for $\alpha\ Pe_m$

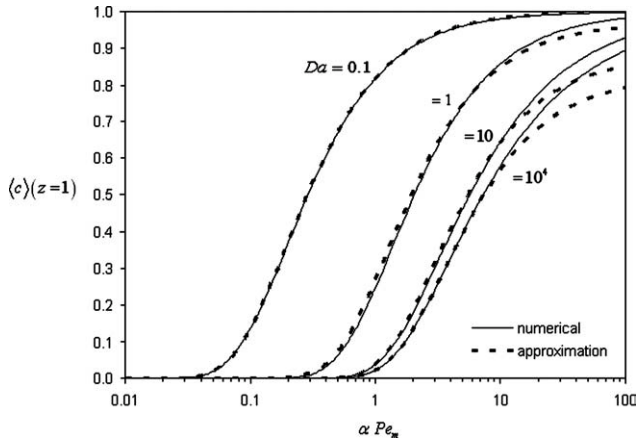

Figure 3. Exit mixing-cup conversion as a function of αPe_m for laminar flow inside a circular channel.

Curves for several values of $Da^* = Da = Da^{II}\,\eta$ are plotted, comparing numerical results (full lines) with approximate 1-term expression (Eq. 11, dashed lines).

< 30 when $Da = 10$, and $\alpha\, Pe_{\rm m} < 20$ when $Da = 10^4$), while parallel plates can be represented correctly at least up to $\alpha Pe_m = 100$ with less than 5% error for $Da \leq 10$ but only up to $\alpha Pe_m = 70$, close to the Dirichlet limit ($Da = 10^4$).

The introduction of the results for w_1 and λ_1 presented in previous sections into Eq. (11) allow us to calculate conversion in a channel directly from the governing dimensionless parameters. However, if explicit approximations to conversion are sought (without going through the eigenvalue and weights dependence relationships), simple expressions for kinetic control conditions and mass transfer controlled conditions can provide useful insight. While in the former case, this yields the well-known result for exponential decrease in the equivalent homogeneous model (e.g., Damköhler[12]):

$$\langle c\rangle(z) \sim \exp\left(\frac{-(j+1)Da}{\alpha Pe_m} z\right) \qquad (Da \ll 1), \qquad (23)$$

for the latter, we obtain

$$\langle c\rangle(z) \sim w_{1,\infty} \exp\left(\frac{-\lambda_{1,\infty}^2}{\alpha Pe_{m,\max}} z\right)\left\{1 + \frac{1}{Da}\left[1 + \frac{(1+j)}{\sigma^2}\lambda_{1,\infty}^4 \frac{z}{\alpha Pe_m}\right]\right\} + O\left(\frac{1}{Da^2}\right) \quad (Da \gg 1). \quad (24)$$

Equation (24) with an $O(1/Da)$ correction to Dirichlet's limit agrees reasonably well with the numerically calculated data from gPROMS®. For instance, for laminar flow in a circular channel and $Da = 20$, Eq. (24) gives less than 4×10^{-4} absolute error for $\alpha\, Pe_m/z < 1$. For $\alpha\, Pe_m/z$ around 1 and up to 20, the approximation predicts less than 2% error. For $Da = 10$, the relative error is near 2% when $\alpha\, Pe_m/z \sim 1$. In the same conditions, maximum error is around 5% for all $\alpha\, Pe_m/z$ higher than 0.65. For $\alpha\, Pe_m/z < 0.65$, the high relative errors correspond to maximum absolute error of 5×10^{-4}, since concentration is getting negligible on this limit.

Eq. (11) with our approximations for λ_1 and w_1, and in particular limits (23) and (24), show the dependence of conversion on the Graetz parameter (the reciprocal of $z/\alpha\, Pe_m$) and on Da, for finite kinetic rates (tending to kinetic and mass transfer controlled limits). Explicit analytical expressions without the need of numerical evaluation for this case have not been presented previously. Bhattacharya et al.[3] present explicit asymptotic expressions to conversion for a parametric range of $P \gg 1$ (their parameter P is equivalent to $\sim \alpha\, Pe_m$) in the Dirichlet ($Da \to \infty$) and Neumann ($Da \to 0$) limits. The applicability of these results in the range of $\alpha\, Pe_m/z \sim 1$ is extremely limited (e.g., more than 20% relative error for $\alpha\, Pe_m < 16$ and $Da = 10$ in round tube with parabolic flow). For a small aspect ratio channel, this merely rewrites Lévêque's regime results, which have been dealt extensively elsewhere.[19,25–27,41,57,58] Therefore, in terms of explicit approximate solutions, the results in this section completes the description of this problem in previous literature, especially in what has been identified[3] as the parameter regime for the optimal design of catalytic monoliths: $P \sim \alpha Pe_m \sim 1$ (e.g., near the mass transfer controlled regime). Moreover, it is possible to identify the effect of design variables on conversion from Eq. (11): (a) the channel length L appears only in the argument of the exponential, showing a steeper increase in conversion for longer channels; and (b) the pre- exponential factor is a decreasing function of the channel transverse length a, but the dominant behavior is given by the increase of the time constant for interphase mass transfer in the denominator of the exponential argument, lowering conversion for channels with larger cross- sections. The influences of the fluid velocity inside the channel and of the bulk diffusivity on conversion are reciprocal to those of L or a, respectively. Finally, both diffusivity and kinetic constants depend on the operating temperature, the latter being usually more sensitive. Naturally, higher temperature leads to a steeper decrease of the mixing-cup concentration, as a result of faster reaction.

Another strategy that we explore next, is the use of Lévêque type corrections (constructed for $\alpha\, Pe_m \gg 1$) to improve the performance at intermediate values of $\alpha\, Pe_m \sim 1$. To our knowledge, the effect of finite reaction rate conditions in these corrections has not been discussed so far.

Lévêque's Regime (Dominant Convection)

At high flow rates ($\alpha\, Pe_m \gg 1$), the transport of reactant towards the walls is now limited by transverse diffusion. If the consumption of reactant at the wall is fast enough, the solution can be decomposed in the transverse direction into two domains: an outer region (which occupies most part of the channel's cross-section, $0 \leq r < 1$) and a concentration boundary layer near $r = 1$ (see Appendix A). In this section, we treat the convection dominated regime as a perturbation problem, allowing us to separate the influence of effects, such as curvature and nonlinearities in the velocity profile (see Appendix B), and identify the parametric conditions where they are relevant, under finite reaction kinetics conditions. Table 1 summarizes some of the previous work invariably associated with Dirichlet and Neumann boundary conditions.

Approximate solution to Lévêque's problem under finite reaction rate conditions

From previous studies (see Table 1), it is clear (especially for laminar flow) that more convenient solutions to the

mixing-cup concentration without requiring numerical evaluation are needed, when Da is finite. As shown in Appendix A, the correct scaling of Eq. (4) includes the thickness of the boundary layer, which is $\delta_R \sim \delta_X \sim (\alpha\ Pe_m)^{-1/2}$ for plug flow and $\delta_X \sim (3\ \alpha\ Pe_m)^{-1/3}$ for laminar flow between parallel plates or $\delta_R \sim (4\ \alpha\ Pe_m)^{-1/3}$ if a parabolic velocity profile inside a circular channel is considered. This results in the appearance of the rescaled Damköhler number, Da^* ($= Da^{II}\ \eta\ \delta_R$).

The conversion can be obtained from surface conditions from

$$\langle c\rangle(z) = \sum_{n=0}^{\infty} \langle c\rangle_n \delta^n, \text{where} \tag{25a}$$

$$\langle c\rangle_0(z) = 1 - \frac{(j+1)Da^*}{\alpha Pe_m \delta} \int_0^z c_0(0,z)dz, \tag{25b}$$

$$\langle c\rangle_n(z) = -\frac{(j+1)Da^*}{\alpha Pe_m \delta} \int_0^z c_n(0,z)dz, \tag{25c}$$

and $j = 0$ or 1 for parallel plates or circular geometry, respectively.

Plug-Flow. For uniform velocity profile $u(R) = \langle u\rangle$, the result for mixing-cup concentration follows immediately from Eq. (25)b and with c_0 (0, z) in Carslaw and Jaeger,[13] we obtain

$$\langle c\rangle_0(z) = 1 - \frac{j+1}{\sqrt{\alpha Pe_m}}\left[\frac{2}{\sqrt{\pi}}\sqrt{z} - \frac{1}{Da^*} + \frac{e^{(Da^*)^2 z}}{Da^*}\text{erfc}(Da^*\sqrt{z})\right] \tag{26}$$

Although an exact solution is provided by Eq. (26), the limits of $Da^* \ll 1$ and $\gg 1$ are of interest:

$$\langle c\rangle_0(z) = 1 - \frac{j+1}{\sqrt{\alpha Pe_m}} \times \left[Da^* z - \frac{4}{3\sqrt{\pi}}(Da^*)^2 z^{3/2} + O(Da^*)^3\right] \quad Da^* \ll 1 \text{ or } z \ll 1 \tag{27a}$$

$$\langle c\rangle_0(z) = 1 - \frac{j+1}{\sqrt{\alpha Pe_m}} \times \left[\frac{2}{\sqrt{\pi}}\sqrt{z} - \frac{1}{Da^*} + \frac{1}{\sqrt{\pi z}}\frac{1}{(Da^*)^2} + O(Da^*)^{-3}\right] \quad Da^* \gg 1 \tag{27b}$$

An approximation to Eq. (26) that "matches" (not in the asymptotic sense) the leading order estimates in Eqs. (27) and still yields a valid estimate even when $Da^* \sim 1$ is obtained next. A rational function that respects both limits is of the form:

$$\langle c\rangle_0(z) = 1 - \frac{j+1}{\sqrt{\alpha Pe_m}}\frac{Da^* z}{1 + \sqrt{\pi}/2\sqrt{z}Da^*}. \tag{28}$$

The exit conversion ($X_c = 1 - \langle c\rangle$ ($z = 1$)) for flow between parallel plates (Figure 4) is well described for a large range of parameters by Eq. (28), with maximum relative errors of 1.4%, 0.4% and 0.1% for $\alpha Pe_m = 10$, 100 and 1000, respectively, all around $Da^* \sim 3$, when compared with numerical results from gPROMS®. These errors can be attributed to the conceived rational approximation, although increase in Péclet number is always beneficial. For $\alpha Pe_m = 1$ (i.e., outside the asymptotic conditions under which this approximation has been developed), less than 1% error is obtained for $Da^* < 1$ (point noted by o in Figure 4).

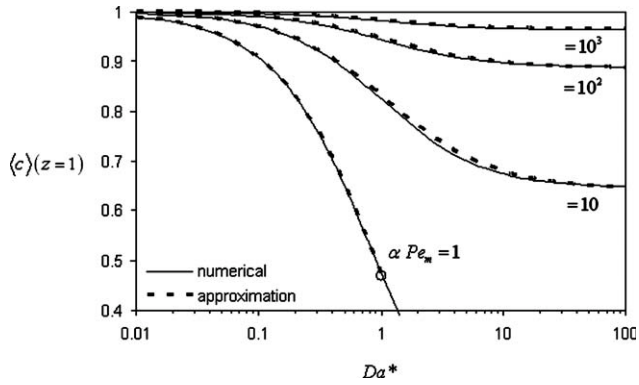

Figure 4. Exit mixing-cup concentration $\langle c\rangle(z = 1)$ as a function of $Da^* = Da^{II}\eta/\sqrt{\alpha Pe_m}$ for several orders of magnitude of αPe_m in plug-flow between parallel plates.

Full lines represent numerical simulation with gPROMS® ($\alpha = 0.01$), while dashed lines refer to Eq. 28.

For plug-flow in a circular channel, the error associated with Eq. (28) has contributions due to the uniform approximation itself, to curvature effects and to finite αPe_m values ("1 term" curve in Figure 5). In general, the relative error can have several local maximums all located at the intermediate range [$\sim$1, due to the nature of approximation (28)] or reasonably high Da^* (due to the ignored curvature effects). In the Dirichlet limit, conversion can be predicted with at most $\sim$0.2% of error for high αPe_m (this is 10 times the value observed for parallel plates geometry). These results suggest that accounting for the presence of curvature may reduce the error in these approximations (in certain ranges of Da^*). Also, for several values of Da^* and αPe_m, the relative errors tend to decrease as we approach the inlet.

Laminar Flow. The degree of reactant's conversion can then be calculated from Eq. (25)b for both limits with the asymptotic expressions for c_0 (0, z) presented in Ghez,[28] yielding

$$\langle c\rangle_0(z) = 1 - \frac{(j+1)Da^*}{\alpha Pe_m \delta}z + 1.1521\frac{(j+1)(Da^*)^2}{\alpha Pe_m \delta}z^{4/3} - 1.2506\frac{(j+1)(Da^*)^3}{\alpha Pe_m \delta}z^{5/3} + O\left(\frac{(Da^*)^4 z^2}{\alpha Pe_m \delta}\right) \text{ for } Da^* z^{1/3} \ll 1, \tag{29a}$$

$$\text{and } \langle c\rangle_0(z) = 1 - 0.8076(j+1)\frac{z^{2/3}}{\alpha Pe_m \delta} + 0.5952\frac{(j+1)}{Da^*}\frac{z^{1/3}}{\alpha Pe_m \delta} \text{ for } Da^* z^{1/3} \gg 1. \tag{29b}$$

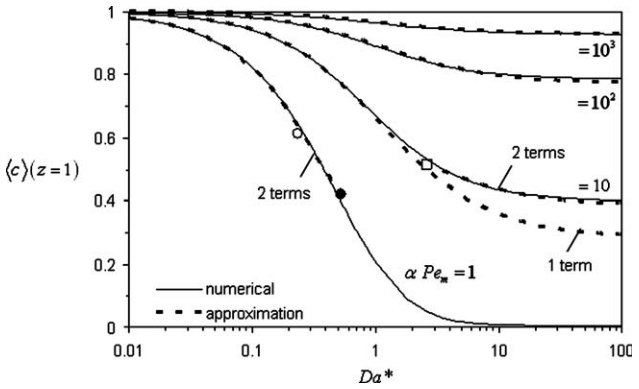

Figure 5. Exit mixing-cup concentration $\langle c\rangle(z = 1)$ as a function of $Da^* = Da^{II}\eta/\sqrt{\alpha Pe_m}$ for several orders of magnitude of αPe_m in plug-flow inside a circular channel.

Full lines represent numerical simulation with gPROMS® ($\alpha = 0.01$), while dashed lines refer to approximate solutions. High values of αPe_m (10^2 and 10^3) are reasonably described by Eq. 28. For $\alpha\ Pe_m = 1$, the 1-term approximation ($\langle c\rangle_0$ from Eq. 28) has less than 5% relative error (up to the point ○) and the 2-term approximation (with $\langle c\rangle_1$ from Eq. 31) provides less than 5% error (up to ●). For $\alpha\ Pe_m = 10$, the high Da^* asymptote second term from Eq. 32 significantly improves the approximation ("2 terms" curve after the point □).

where $Da^* = Da^{II}\ \eta\ \delta$, where δ has different definitions according to the geometry and flow profile. When compared with the numerical solution of the full model (from gPROMS®), the $O(Da^{*2})$ and $O(Da^{*-1})$ approximations (obtained truncating Eqs. (29) only to leading-order dependence on z) are rather limited in applicability, specially for a circular channel geometry. However, we note that a rational expression (similar to Eq. (28)) bringing together the solution for small and large values of $Da^*\ z$, may actually perform better than (or at least, comparably with) the individual limits it is meant to fulfill:

$$\langle c\rangle_0(z) = 1 - \left(\frac{j+1}{\alpha Pe_m\delta}\right)\frac{Da^* z}{1 + 1.2382 Da^* z^{1/3}}. \qquad (30)$$

Eq. (30) predicts conversion in a circular channel with around 1.4% error for $\alpha Pe_m = 100$ and ~0.13% for $\alpha Pe_m = 1000$, as Da^* increases. For slit channels though, the exit mixing-cup conversion can be reasonably calculated over large parametric ranges (Figure 6). For example, up to the Dirichlet limit (large Da^*) maximum relative errors are: 3% for $\alpha Pe_m = 10$, ~ 0.1% for $\alpha Pe_m = 100$ and ~ 0.01% for $\alpha Pe_m = 1000$. In this case, even when $\alpha Pe_m = 1$, less than 5% error is achieved for $Da^* < 0.5$. The effect of curvature clearly reduces the accuracy of the approximations (mainly for finite (moderate) values of αPe_m), which stresses the importance of a curvature correction.

Effect of curvature in a circular channel with plug flow

The results of interest (check Appendix B for details) are the limits of low and high Da^* of the mixing-cup concentration which according to Eq. (25)c are:

$$\langle c\rangle_1(z) = \frac{(Da^*)^2}{\alpha Pe_m\delta}\left(\frac{z^2}{2} - \frac{16 z^{5/2}}{15\sqrt{\pi}} Da^*\right) + O(Da^{*4}) \quad \text{for } Da^* \ll 1 \qquad (31)$$

$$\langle c\rangle_1(z) = \frac{z}{\alpha Pe_m\delta}\left(1 - \frac{4}{\sqrt{\pi z}}\frac{1}{Da^*}\right) + O(Da^{*-2}) \quad \text{for } Da^* \gg 1. \qquad (32)$$

From the previous numerical results, we saw that this correction is mainly needed for $Da^* \gg 1$ (note that for $Da^* \ll 1$, the correction is of $O(Da^{*2})$). The "curvature correction" can be simplified to $\langle c\rangle_1(z) \sim \frac{z}{\alpha Pe_m\delta}$, only when $Da^* \gg 1$.

The high Da^* asymptote in Eq. (32) improves the approximation even at moderate values (□ in Figure 5). In particular for $Da^* = 100$, the error drops an order of magnitude: from 27% to 1.5% ($\alpha\ Pe_m = 10$), from 1.29% to 0.02% ($\alpha\ Pe_m = 100$) and from 0.14% to 0.03% ($\alpha\ Pe_m = 10^3$). The low Da^* term (Eq. (31)) is more useful for $\alpha\ Pe_m = 1$ to extend the validity of the approximate solution given by Eq. (28) from $Da^* < 0.2$ (limit shown by ○) to $Da^* < 0.5$ (limit shown by ●), with maximum 5% relative error compared to numerical results.

The contribution of curvature $\delta\langle c\rangle_1$ is more significant at high Da^* and is less than 1% of $\langle c\rangle_0$ for $\alpha\ Pe_m/z \geq 100$, however it is less than 30% of $\langle c\rangle_0$ for $\alpha\ Pe_m/z \geq 10$.

Effect of nonlinear velocity profile in laminar flows

In this case (see Appendix B for details), the higher order correction writes in the limits of high and low Da^* as

$$\langle c\rangle_1(z) \sim 0.125\frac{(1+j)}{\alpha Pe_m\delta}(Da^*)^2 z^{5/3} + O(Da^{*3}) \qquad \text{for } Da^* \ll 1 \qquad (33)$$

$$\langle c\rangle_1(z) \sim \frac{(1+j)z}{10\alpha Pe_m\delta}\left(1 - \frac{1.615 z^{-1/3}}{Da^*}\right) + O(Da^{*-2}) \quad \text{for } Da^* \gg 1. \qquad (34)$$

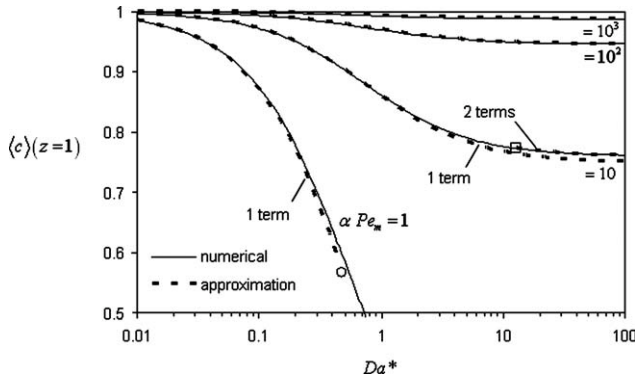

Figure 6. Exit mixing-cup concentration $\langle c\rangle(z = 1)$ as a function of $Da^* = Da^{II}\eta/(3\alpha\ Pe_m)^{1/3}$ for several orders of magnitude of $\alpha\ Pe_m$ for laminar flow between parallel plates.

Full lines represent numerical simulation with gPROMS® ($\alpha = 0.01$), while dashed lines refer to approximate solutions. One-term solutions are given by Eq. 30, to which a correction accounting for velocity profile nonlinearity (first term in Eq. 34) is added so that a two-term approximation is conceived ("2 terms" curve after □).

Again for low Da^*, the contribution is of $O(Da^{*2}/(\alpha\ Pe_m\ \delta))$ and therefore negligible. However, in the limit of high Da^*, the correction is more significant.

Parallel Plates. Two terms in Eq. (34) should be retained in the ranges of $1.8 < Da^* < 12$, $4.4 < Da^* < 20$ and $0.75 < Da^* < 26.5$ for $\alpha\ Pe_m = 10$, 100, and 10^3 (with respective maximum relative errors of 0.20%, 0.03% and 0.009%, respectively). In particular for $Da^* = 100$, errors are reduced by one order of magnitude comparing to the ones obtained with (30). For $\alpha\ Pe_m = 10$, $\langle c\rangle_0(z)$ reasonably describes numerical solutions up to $Da^* = 12.7$ (shown in Figure 6 by □). For $\alpha\ Pe_m = 1$, results with less than 5% error are obtained for $Da^* < 0.5$ with $\langle c\rangle_0(z)$ from Eq. (30) (○ in Figure 6).

Circular Channel. At low Da^*, the improvement brought by Eq. (33) is not particularly visible, as for $\alpha\ Pe_m = 1$, the error is already less than 5% for $Da^* < 0.1$ (o in Figure 7). Eqs. (33) and (34) result in improvement of the rational function for $\langle c\rangle_0$ (Eq. (30)) with transition between asymptotes around $Da^* \sim 1$. The effect of correction (34) at $Da^* = 100$ is quite modest. When $\alpha\ Pe_m$ is not high enough and Da^* is large, the Graetz solution is more appropriate to describe accurately the numerical results. In this case (finite $\alpha\ Pe_m$), the penetration of concentration gradients is visible at a length scale comparable to the channel characteristic dimension a, much thicker than $a\ \delta_R$. The leading order solution at low Da^*, given by the first couple of terms in Eq. (29), can be connected to Graetz's estimate at the Dirichlet limit (Eq. (11)) with error slightly above 2% for $Da^* = 100$. Such approximation is plotted in Figure 7 for $\alpha\ Pe_m = 10$ and writes as:

$$\langle c\rangle(1) \sim 1 - \frac{(j+1)Da^*}{\alpha Pe_m \delta} \frac{w_{1,\infty} \exp\left(\frac{-\lambda_{1,\infty}^2}{\alpha Pe_{m,\max}}\right)}{1 + \frac{(j+1)Da^*}{\alpha Pe_m \delta} - w_{1,\infty} \exp\left(\frac{-\lambda_{1,\infty}^2}{\alpha Pe_{m,\max}}\right)}. \tag{35}$$

As shown in Figures 4–7 and in the previous discussion, the extended Lévêque solutions improve the prediction of conversion significantly even at the exit of the channel. Here, the flow can be already fully developed, so corrections due to velocity profile nonlinearity are important. Improvement resulted for values of $\alpha\ Pe_m$ as low as 10.

Kinetic Normalization for "Power-Law" Reaction Rates

When reactions are unimolecular or when all reactants (species i) except one are present in excess, $\mathcal{R}\{c_i(r=1,z)\} = \mathcal{R}\{c(r=1,z)\}$. Moreover, if reactant concentration is kept in a restricted range, the so-called "power-law kinetics" can be used as a reasonable approximation to the actual rate equation: $\mathcal{R}\{c(r=1,z)\} = k_{\text{surf}} c^m(r=1,z)$, where m is the order of reaction. Concerning the coupled analysis of (channel) flow past a surface where a reaction with arbitrary kinetics is occurring, a great deal of work exists (see Table 1). A generic approximate approach to convective-transport problems past catalytic surfaces is to reduce the problem (Lighthill transformation[60]) to an integral equation relating surface concentration and reaction rate integral equation method), which is usually solved numerically. Bhattacharya et al.[3] present numerical results for power law kinetics (of orders $m = 1/2$, 1, and 2) for plug flow in a short monolith channel and also for some types of Langmuir-Hinshelwood kinetics (with multiplicity behavior). They observed that the same asymptotes for kinetic and mass transfer controlled limits were fulfilled.

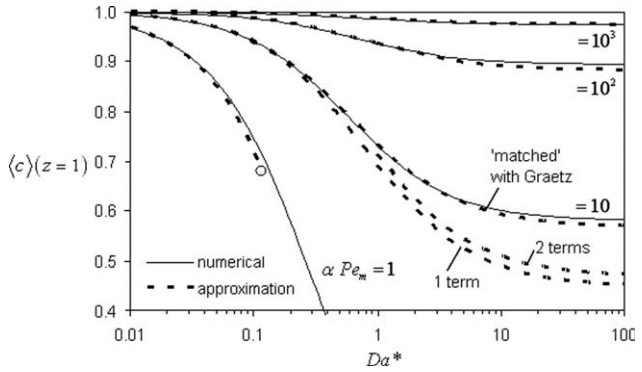

Figure 7. Exit mixing-cup concentration $\langle c\rangle(z = 1)$ as a function of $Da^* = Da^{II}\ \eta/(4\alpha Pe_m)^{1/3}$ for several orders of magnitude of αPe_m for laminar flow inside a circular channel.

Full lines represent numerical simulation with gPROMS® ($\alpha = 0.01$), while dashed lines refer to approximate solutions. One-term solutions are given by Eq. 30, to which a correction accounting for nonlinear velocity profile is added so that a two-term approximation is conceived ("2 terms" curve). Eq. 35 is also plotted for $\alpha Pe_m = 10$, when Lévêque's leading-order results arc 'matched' with Graetz's one-term approximation.

In this section, we extend our approximations in fully developed Graetz and Lévêque's regimes to "power-law" kinetics. Our objectives are the following: (a) to obtain explicit formulas for conversion under kinetic and mass transfer control, and (b) to understand the influence of the reaction rate law through calculation of higher-order contributions in suitable limits.

Developing concentration profile

When the concentration profile is developing, the rescaled wall boundary condition for the nonlinear problem is:

$$\left.\frac{\partial c}{\partial R}\right|_{R=0} = Da^* c^m(R=0,z) \quad (\text{power} - \text{law kinetics}) \tag{36}$$

In Eq. (36), the Da^* parameter is defined as usual in Lévêque's regime with the thickness of the boundary layer ($= Da^{II}\ \eta\ \delta_R$), however k_{surf} is replaced by $\mathcal{R}_{\text{surf}}(\hat{c}_{in})/\hat{c}_{in}$. To obtain approximate solutions, we must reduce the boundary condition by choosing Da^* (or its reciprocal) as perturbation parameter ε. This will not result in any simplification of the complete mass balance in the channel, which is free of ε. Therefore, we start by analyzing Lévêque's regime, where a set of assumptions for $\delta_R \sim (\alpha\ Pe_m)^{-q} \ll 1$ ($q = 1/2$ for plug flow and $q = 1/3$ for laminar flow) allows simplification of the mass balance to Eqs. (A1).

We consider a perturbation series for concentration with the following form

$$c(R,z;\varepsilon) = \sum_{n=0}^{\infty} c_n(R,z)\delta_n(\varepsilon) \tag{37}$$

where, $c_n(R,z)$ is the solution to the n^{th} subproblem (of $O(\delta_n)$), ε is the small parameter (which can be either $\varepsilon = Da^*$ for kinetic control or $\varepsilon = 1/Da^*$ for mass transfer control) and $\delta_n(\varepsilon)$ are undetermined gauge functions of ε, which will be defined by convenient dominant balances, obeying the following relation $\delta_n(\varepsilon) \gg \delta_{n+1}(\varepsilon)$ as $\varepsilon \to 0$.

The subproblems appearing after introducing (37) into the leading-order problem from Eq. (A1) and collecting the same order terms are

$$\frac{\partial^2 c_n}{\partial R^2} = \frac{\partial c_n}{\partial z} \quad \text{(plug flow)} \tag{38a}$$

$$\frac{\partial^2 c_n}{\partial R^2} = R\frac{\partial c_n}{\partial z} \quad \text{(laminar flow)}. \tag{38b}$$

Since our perturbation to boundary condition (36), associated with the nonlinear kinetics, will render the problem linear, Eqs. (38) are amenable to be treated with Laplace transform of $u_n(R,z) = c_n(R,z) - c_n(R,0)$ with respect to z, yielding the following general solutions for the n^{th} subproblem

$$\overline{u}_n(R,s) = const\ e^{-R\sqrt{s}} \quad \text{(plug flow)} \tag{39a}$$

$$\overline{u}_n(R,s) = const\ \mathrm{Ai}(R\ s^{1/3}) \quad \text{(laminar flow)}. \tag{39b}$$

Note that $c_n(R,0) = 1$ for $n = 0$ but $c_n(R,0) = 0$ for $n \geq 1$, and therefore $\overline{u}_n(R,s) = \overline{c}_n(R,s)$ (for $n \geq 1$). Solutions (39) were obtained so that boundedness as $R \to \infty$ is achieved.

The mixing-cup can be written as

$$\langle c \rangle(z) = 1 - \frac{(j+1)}{\alpha Pe_m \delta} \sum_{n=0}^{\infty} \langle c \rangle_n \delta_n(\varepsilon), \tag{40}$$

where the contributions from the $O(\delta_n)$ subproblems are

$$\langle c \rangle_n(z) = \int_0^z \left.\frac{\partial c_n}{\partial R}\right|_{R=0} dz = \mathcal{L}^{-1}\left\{\frac{1}{s}\left.\frac{d\overline{c}_n}{dR}\right|_{R=0}\right\}. \tag{41}$$

Kinetically Controlled Regime. If we seek for a perturbation solution in $\varepsilon = Da^*$, the wall boundary condition (36) after introduction of Eq. (37) becomes,

$$\sum_{n=0}^{\infty} \left.\frac{\partial c_n}{\partial R}\right|_{R=0} \delta_n = \varepsilon \left(\sum_{n=0}^{\infty} c_n(0,z)\delta_n\right)^m \quad \text{(power law kinetics)} \tag{42}$$

As both wall concentration and flux are correctly scaled, the left-hand side of (42) is dominant and therefore the leading order term is unbalanced by any term of the right hand side as $\varepsilon \to 0$, i.e.,

$$\left.\frac{\partial c_0}{\partial R}\right|_{R=0} \delta_0(\varepsilon) = 0 \text{ from where } \left.\frac{\partial c_0}{\partial R}\right|_{R=0} = 0 \tag{43}$$

and for convenience, $\delta_0(\varepsilon) \sim 1$. The solution of Eqs. (39) subject to (43) is, as expected,

$$c_0(R,z) = 1. \tag{44}$$

The next subproblem is defined by Eqs. (38) with $n = 1$ and must be solved with the boundary condition given by

$$\left.\frac{\partial c_1}{\partial R}\right|_{R=0} = c_0^m = 1. \tag{45}$$

Here, the dominant balance is between the second higher term in the LHS and the higher in the RHS of Eq. (42), of order $\delta_1 \sim \varepsilon\delta_0$. Up to this order, Lévêque's problem with uniform wall flux is reproduced and for zero-order reactions with nonzero wall concentration, no further corrections from higher subproblems exist. Also so far, the presence of the order of reaction m is not felt, apart from the parameters definition. An higher order kinetics-dependent term is calculated from

$$\left.\frac{\partial c_2}{\partial R}\right|_{R=0} = m\ c_1(0,z) \quad \text{(power law kinetics)}, \tag{46}$$

where $c_2(R,z)$ is the solution at order $\delta_2 \sim \varepsilon^2$. Note that the form of our perturbation expansion, in integer powers of ε ($\delta_n \sim \varepsilon^n$) is independent of m. The Laplace transform of the flux towards the wall is given by

$$\left.\frac{\partial \overline{c}_2}{\partial R}\right|_{R=0} = m\ \overline{c}_1(0,s) = -ms^{-3/2} \quad \text{(plug flow)} \tag{47a}$$

$$\left.\frac{\partial \overline{c}_2}{\partial R}\right|_{R=0} = m\ \overline{c}_1(0,s) = \frac{\mathrm{Ai}(0)}{\mathrm{Ai}'(0)} ms^{-4/3} \quad \text{(laminar flow)}. \tag{47b}$$

According to the previous results and from Eqs. (40)–(41):

$$X_R(z) = \frac{(j+1)}{\alpha Pe_m \delta}\left[zDa^* - \frac{4}{3\sqrt{\pi}} mz^{3/2} Da^{*2} + O(Da^{*3})\right] \text{ (plug flow)}. \tag{48a}$$

$$X_R(z) = \frac{(j+1)}{\alpha Pe_m \delta}\left[zDa^* - 1.15209\ mz^{4/3} Da^{*2} + O(Da^{*3})\right] \text{ (laminar flow)}. \tag{48b}$$

The well-known solutions for first and zero-order reactions are recovered from Eqs. (48). The same order terms in Eqs. (27) and (29) are reproduced for $m = 1$, while $\langle c \rangle_2(z) = 0$ for $m = 0$. For the general case of an m^{th} order reaction, more subproblems could be generated and solved in a similar way, however terms up to $O(Da^*)^2$ are enough for our purposes, since the effect of m has already been captured. This term is the basis of the normalization for kinetic control when the concentration profile is developing with respect to the reaction rate exponent m. When flow profile is fully developed in a circular channel (the worst case possible for Lévêque's leading-order problem with linear wall velocity profile and negligible curvature assumptions), the inclusion of $\langle c \rangle_2(z)$ improves the estimate from (40) reducing relative errors for $Da^* \sim 0.1$ by about one order of magnitude. In this example, when $m = 1/2$ the maximum relative error for $Da^* \leq 0.1$ reduces from 0.1% to 0.02%,

while when $m = 1$ the drop in error is between 0.2 and 0.004%. Finally, for $m = 2$ the predicted error of 0.4% is reduced to less than 0.06%, when our analytical results are compared with numerical simulations in gPROMS® for $\alpha\, Pe_m = 100$.

External Mass Transfer Controlled Regime. In the limit of instantaneous reaction at the catalytic surface, we take the perturbation parameter as $\varepsilon = 1/Da^*$ and at leading order ($n = 0$) obtain the Dirichlet problem, given by the $O(1)$ terms in Eqs. (27)b and (29)b. This happens since the RHS in Eq. (36) is not balanced by any term in the LHS and we set $\delta_0 \sim 1$. So, at leading order the problem is again independent of the specific form of reaction kinetics, as concentration vanishes at the wall for any form of $\mathcal{R}(c)$. We now follow to calculate an higher order term in this limit.

The form of the perturbation expansion and the appropriate form of the wall boundary condition for the next subproblem are determined by introducing (37) into (36):

$$\sum_{n=1}^{\infty} c_n(0,z)\delta_n = \left(\varepsilon \sum_{n=0}^{\infty} \left.\frac{\partial c_n}{\partial R}\right|_{R=0} \delta_n\right)^{1/m} \quad \text{(power law kinetics)} \tag{49}$$

Requiring the next term in the LHS to balance with the highest in the RHS yields $\delta_1(\varepsilon) \sim \varepsilon^{1/m}$, with $m > 0$ so that $\delta_1(\varepsilon) \to 0$ as $\varepsilon \to 0$. The boundary condition becomes

$$c_1(0,z) = \left(\left.\frac{\partial c_0}{\partial R}\right|_{R=0}\right)^{1/m} \quad \text{(power law kinetics)}. \tag{50}$$

If Eq. (49) is expanded for small δ_n and terms organized by order of magnitude it is possible to show that the consistent choices for the form of perturbation series (37) are of the form: $\delta_n(\varepsilon) \sim \varepsilon^{n/m}$, for power law kinetics of order m. Note that, as dictated by the dominant balance, the form of the series in dependent on the reaction order in this case. Therefore, subsequent corrections to the leading order term will vanish faster (for the same Da^*) if $m < 1$. For $m = 0$, no corrections to Dirichlet's limit exist, as expected in conditions of reactant exhaustion at the wall.

At $O(\varepsilon^{1/m})$, the particular solutions according to (39) subject to Eq. (50) are

$$\overline{c}_1(R,s) = s^{\frac{-1}{2m}} e^{-R\sqrt{s}} \quad \text{(plug flow)} \tag{51a}$$

$$\overline{c}_1(R,s) = \left[\frac{\Gamma(2/3)}{3^{2/3}\Gamma(4/3)}\right]^{1/m} s^{-\frac{2}{3m}} \frac{\mathrm{Ai}(Rs^{1/3})}{\mathrm{Ai}(0)} \quad \text{(laminar flow)}. \tag{51b}$$

The respective contributions for mixing cup concentrations are calculated from Eq. (41):

$$\langle c\rangle_0(z) = \frac{2\sqrt{z}}{\sqrt{\pi}} \quad \text{(plug flow)} \tag{52a}$$

$$\langle c\rangle_0(z) = \frac{\Gamma(2/3)z^{2/3}}{3^{2/3}\Gamma(4/3)\Gamma(5/3)} = 0.807549 z^{2/3} \quad \text{(laminar flow)} \tag{52b}$$

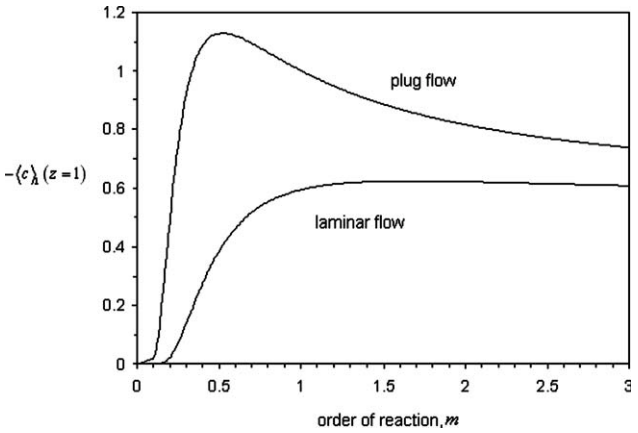

Figure 8. Contribution of $O(Da^*)^{-1/m}$ term at the exit of a channel (with plug or laminar flow), as a function of the reaction order m, Eqs. 53.

$$\langle c\rangle_1(z) = -\frac{z^{\frac{1}{2m}-\frac{1}{2}}}{\Gamma\left(\frac{1}{2}+\frac{1}{2m}\right)} \quad \text{(plug flow)} \tag{53a}$$

$$\langle c\rangle_1(z) = \frac{-3^{\frac{1}{3}-\frac{2}{3m}}\Gamma(2/3)^{1+1/m}}{\Gamma(1/3)\Gamma(4/3)^{1/m}} \frac{z^{\frac{2}{3m}-\frac{1}{3}}}{\Gamma\left(\frac{2}{3m}+\frac{2}{3}\right)} \quad \text{(laminar flow)}. \tag{53b}$$

Eqs. (52) are the well-known results from the Dirichlet limit.[14,42] The inversion of Laplace transforms in Eqs. (53) is acceptable for $m > 0$. For $m = 1$, the $O(Da^*)^{-1}$ term in Eqs. (27)b and (29)b is reproduced. The $-\langle c\rangle_1$ ($z = 1$) contribution is plotted in Figure 8 as a function of the order of reaction m. The behavior for plug and laminar flows is slightly different, and the effect of changing m is more pronounced in the former.

The contribution to conversion given by $\langle c\rangle_1$ ($z = 1$) $(Da^*)^{-1/m}$ is more important for $m > 1$. For laminar flow in a round tube ($\alpha\, Pe_m = 100$), the two-term perturbation solution for conversion predicts less than 1.5% of relative error for $Da^* > 1$ when $m = 1/2$ and 1, which is comparable to the errors from Eq. (30). However, for $m = 2$ the error involved in the use of rational approximation (30) is reduced to half by adding the term in (53)b, yielding less than 2% relative error for $Da^* > 1$. Figure 9 illustrates the improvement in the approximation for $m > 1$ in comparison with the leading-order result (accounted for in Eq. (30)).

We note that extended Lévêque solutions in the Dirichlet limit (kinetics-independent) can still be used to improve approximations at high Da^*, as shown previously. Also, since the kinetic and external mass transfer regimes are the same, the correlations given by Eqs. (28) and (30) should be generally valid. However, as we see here, a subdominant contribution accounting for kinetics ($O(Da^*)^{-1/m}$, in particular when $m > 1$) can be beneficial for the approximation. For a given axial position z, Eqs. (53) depend only on m and are the basis of our kinetic normalization in the developing mass transfer controlled concentration profile. A simplified analysis of Langmuir kinetics and its relationship with the previous results for 'power law kinetics' is presented in Appendix C.

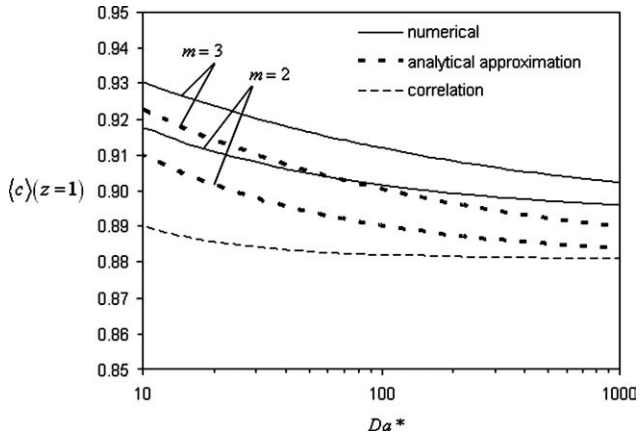

Figure 9. Exit mixing-cup conversion $\langle c \rangle$ ($z = 1$) for laminar flow in a circular channel with power law wall kinetics of order $m = 2$ and $m = 3$ as a function of Da^*.

Full lines correspond to gPROMS® simulations with $\alpha Pe_m = 100$. Thick dashed lines represent the perturbation solution for conversion with the extra term given by Eq. (53) b. Eq. (30), which reasonably describes lower m kinetics, is also shown (thin dashed line).

Fully developed concentration profile

We now consider the case where the solution is given by Graetz series and, in particular, when the first term in this series is dominant (i.e., fully developed concentration profile).

In the kinetic and mass transfer controlled limits, the problem is reduced to the well-known cases of heat transfer in tubes with uniform wall flux or temperature. These will be the starting points to build our approximations for power-law kinetics in both regimes, as shown later.

The boundary condition in the higher order subproblems requires a specified wall flux or concentration distribution to be fulfilled. From studies of heat transfer in ducts, it is known that one can deal with arbitrary wall temperature or flux distributions by superposition of fundamental solutions (of Dirichlet and Neumann types). This procedure has been applied to the Graetz problem by several authors.[13,15,17,21,33,60] We will use the same technique to account for the effect of the kinetic rate expression.

Kinetically Controlled Regime. When reaction is infinitely slow, the mixing-cup and wall concentration are given by $\langle c \rangle_0 (z) = 1$. Instead of using $c_0 (1,z) = 1$ as $O(1)$ solution, we will adopt Eq. (23) to improve our perturbation procedure,

$$c_0(1,z) = \exp\left(\frac{-\sigma Da}{\alpha Pe_{m,\max}} z\right) \quad (Da \ll 1). \tag{54}$$

For power-law kinetics, the first correction that can be calculated is of $O(Da)$ and obeys to Eqs. (1) with the boundary condition:

$$\left.\frac{\partial c_1}{\partial r}\right|_{r=1} = -c_0^m(1,z) = -\exp\left(\frac{-m\sigma Da}{\alpha Pe_{m,\max}} z\right). \tag{55}$$

The mixing-cup average calculation at this order can be calculated directly from (55), according to

$$\frac{d\langle c \rangle_n}{dz} = \frac{j+1}{\alpha Pe_m} \left.\frac{\partial c_n}{\partial r}\right|_{r=1} \text{ and } \langle c \rangle_n (0) = 0 \quad (n \geq 1). \tag{56}$$

In terms of conversion of reactant, $X_R = 1 - \langle c \rangle = 1 - \langle c \rangle_0 - \langle c \rangle_1 \varepsilon + O(\varepsilon^2)$, the following normalization under fully developed kinetic control arises:

$$m X_R = 1 - \exp\left(\frac{-m(j+1)Da}{\alpha Pe_m} z\right). \tag{57}$$

Naturally, these results reduce to Eq. (23) when $m = 1$ and the correction ceases to exist when $m = 0$, where the constant flux asymptote is the exact solution (no wall concentration annulment). In Figure 10, the relationship between mDa and $m X_R$ is plotted for several power-law kinetics in laminar flow at the exit of a circular channel ($j = 1$). It is possible to see that Eq. (57) describes reasonably well all kinetics at least up to $Da \sim 0.1$, even though the curves deviate faster from our approximation as m gets lower. For $Da \leq 0.1$, the maximum relative error between numerical and analytical results are: 1% for $m = 2$, 1.6% for $m = 1$, 0.6% for $m = 1/2$ and 0.5% for $m = 1/3$. Further increasing Da results in bigger deviations for the lower values of m. For lower values of $Da/\alpha\ Pe_m$, maximum relative errors are reduced (e.g., for $Da/\alpha\ Pe_m = 0.01$, to 0.1% for $m = 1$ and 2, and to 0.01% for $m = 1/2$ and 1/3).

External Mass Transfer Controlled Regime. For fast wall reaction rates, the leading order problem (obtained by setting $\varepsilon = 1/Da = 0$ in the boundary condition) admits Graetz's constant wall temperature solution, $c_0(r,z)$. We will assume that for $\partial c_0/\partial r|_{r=1}$ in fully developed concentration profile conditions, the first term in the series is enough. The next subproblem appears at $O(\varepsilon^{1/m})$, as before, and the appropriate wall boundary condition requires an exponential variation of surface concentration given by

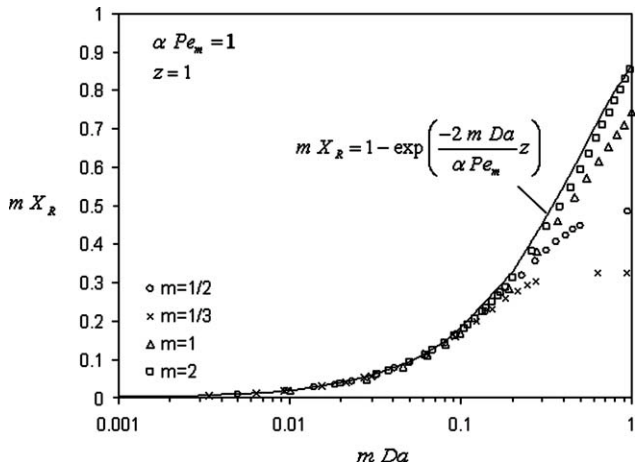

Figure 10. Reactant conversion as a function of Da, for different orders of reaction m.

Comparison between analytical prediction (57) (line) and numerical results (points). The results refer to laminar flow inside a circular channel with $\alpha\ Pe_m/z = 1$.

$$c_1(1,z)=\left[-\left.\frac{\partial c_0}{\partial r}\right|_{r=1}\right]^{1/m}=\left(\frac{w_{1,\infty}\lambda_{1,\infty}^2}{\sigma}\right)^{1/m}\exp\left(\frac{-\lambda_{1,\infty}^2}{m\alpha Pe_{m,\max}}z\right). \tag{58}$$

Since the mass balance is free of the small parameter, $c_1(r,z)$ is still governed by Eq. (1), which is linear. Consider the fundamental solution for a finite step in wall concentration at the inlet (c_{wall}), is given by Graetz's solution with Dirichlet boundary condition:

$$c_{1,\infty}(r,z)=\frac{c_{wall}-c_1(r,z)}{c_{wall}}=\sum_{n=1}^{\infty}A_{n,\infty}\varphi_{n,\infty}(r)\exp\left(\frac{-\lambda_{n,\infty}^2 z}{\alpha Pe_{m,\max}}\right). \tag{59}$$

In the definition from Eq. (59), $c_{1,\infty}(r,\ 0)\ =\ 1$ and $c_{1,\infty}(1,\ z)\ =\ 0$ (which are the usual boundary conditions, since the inlet condition is independent of the small parameter and thus $c_1(r,0) = 0$).

A solution can now be obtained by superposition of several constant-wall temperature steps (equivalent to Duhamel's principle). The flux towards the wall (which is what we need for calculating the velocity-averaged concentration) can be written as an ordinary Reimann integral, plus a summation with contributions for discontinuous steps.[21] For our case,

$$-\left.\frac{\partial c_1}{\partial r}\right|_{r=1}=\int_0^z\left.\frac{\partial c_{1,\infty}}{\partial r}\right|_{r=1,z-z'}\frac{dc_1(1,z')}{dz'}dz'+\left.\frac{\partial c_{1,\infty}}{\partial r}\right|_{r=1}\left(\frac{w_{1,\infty}\lambda_{1,\infty}^2}{\sigma}\right)^{1/m}, \tag{60}$$

where $c_{1,\infty}$ is reaction kinetics independent (Eq. (59)), $c_1\ (1,z)$ is given by Eq. (58) and a 'jump' of magnitude $c_1(1,0)$ is considered at $z = 0$. The respective contribution to the mixing cup concentration profile can be calculated from Eq. (56). From the two first perturbation terms, the mixing-cup concentration profile writes as

$$\langle c\rangle(z)=w_{1,\infty}\exp\left(\frac{-\lambda_{1,\infty}^2 z}{\alpha Pe_{m,\max}}\right)\left\{1+\frac{m}{m-1}\left(\frac{w_{1,\infty}\lambda_{1,\infty}^2}{\sigma Da^*}\right)^{1/m}\left[\exp\left(\frac{m-1}{m}\frac{\lambda_{1,\infty}^2 z}{\alpha Pe_{m,\max}}\right)-1\right]\right\}+O(Da^*)^{-2/m}\quad(Da^*\gg 1). \tag{61}$$

Recall from the "Graetz-Nusselt regime" section, $w_{n,\infty}\lambda_{n,\infty}^2/\sigma = 2$ for plug-flow and $w_{n,\infty}\lambda_n^2/\sigma = 2.02557\ \lambda_n^{-1/3}$ for laminar flow, both $O(1)$ for $n = 1$. When $m = 1$, Eq. (61) agrees with Eq. (24) if estimating w_1 by $w_{1,\infty}$ in the second term is acceptable.

Eq. (61) states that the mixing-cup concentration equals the one observed when reactant exhaustion occurs near the wall multiplied by a corrective function dependent on the order of reaction m, the parameters Da and $\alpha\ Pe_m$, and kinetic rate-independent parameters, such as eigenvalues and weights. This function reduces to unity at the Dirichlet limit, and therefore normalizes our results for developed concentration profile at high Da.

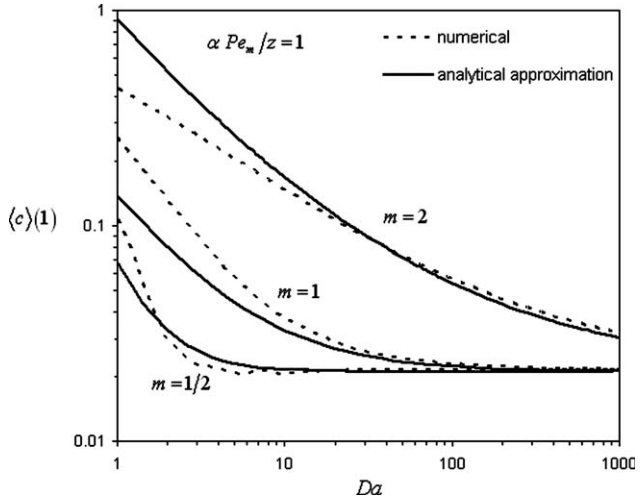

Figure 11. Exit concentration as a function of *Da*, for different orders of reaction *m*.

Comparison between numerical and analytical results. For $m = 2$, the term given by Eq. 64 is included in the analytical result (61). The results refer to laminar flow inside a circular channel with $\alpha\ Pe_m/z = 1$.

As we already recognized for the case of developing concentration profile, the corrections in this perturbation series vanish faster for $m < 1$ as $\varepsilon \to 0$. For higher orders of reaction, an extra term may be calculated in a simplified form, as detailed later.

At $O(\delta_2)$, the balance between terms in the wall boundary condition yields,

$$\delta_2 \sim \varepsilon^{2/m} \sim Da^{-2/m},\ \text{and} \tag{62}$$

$$c_2(1,z)=-\frac{c_1^{m-1}}{m}\left.\frac{\partial c_1}{\partial r}\right|_{r=1}. \tag{63}$$

The problem can be solved for $\langle c\rangle_2$ by the procedure detailed earlier. For fully developed flow and high m, the following simplified result can be obtained:

$$\langle c\rangle_2=\frac{2}{3}\frac{\lambda_{1,\infty}^4 w_{1,\infty}^3}{m\sigma^2}\qquad(m>1). \tag{64}$$

The term given by (64) can then be added to Eq. (61) as $\delta_2\langle c\rangle_2$. Figure 11 compares numerical results for the exit conversion in a circular channel with laminar flow for $\alpha\ Pe_m = 1$ with the previous predictions. For $m = 1/2$, less than 5% relative error is observed for $Da > 6$ and the maximum error is around 2% for $Da > 10$. For first-order reactions, the error is near 5% for $Da > 30$, but if $\langle c\rangle_2$ is included this value drops to 3% for $Da > 20$. Second-order reactions clearly benefit from the estimate in Eq. (64), as a maximum error around 5% is obtained for $Da > 20$, while 20%

relative deviation would have been predicted had the contribution from Eq. (64) been ignored.

Conclusions

This work provides an approximate convenient methodology for the design of microchannel wall-coated reactors. The results presented show that it is possible to describe approximately with analytical techniques the behavior of a small aspect ratio microchannel ($\alpha \ll 1$) with a first-order reaction occurring at the walls, for all values of the rescaled Damköhler number (Da^*) and transverse Péclet number (Pe_m). Solutions to Graetz's problem are provided, with dependence of eigenvalues and weights on Da ($= Da^*$). This allows conversion calculation with no numerical evaluation in commonly encountered practical conditions ($\alpha\ Pe_m \sim O(1)$). Lévêque's regime is treated as a perturbation problem with an uniformly valid leading-order result (over the whole range of Da^* values), followed by corrections accounting for the effect of finite reaction rates in the following contributions: curvature in a circular channel and nonlinear velocity profile in the case of laminar flows. Both higher-order terms proved to be necessary when Da^* is high, and extended Lévêque's results, in some cases at the exit, even when $\alpha\ Pe_m \sim O(1)$.

In the last section, we present normalized results for a power law reaction rate expression. The mixing-cup concentration in the kinetic and mass transfer controlled limits, for both developed and developing profiles, was calculated.

Acknowledgments

J. P. Lopes gratefully acknowledges the financial support from FCT - Fundação para a Ciência e a Tecnologia, PhD fellowship SFRH/BD/36833/2007.

Notation

a = radius of the circular channel or half-spacing between parallel plates
A_n = nth integration constant
$Ai(x)$ = Airy function
b = exponent in Eq. 22
c = bulk fluid concentration of reactant species
$\langle c \rangle$ = reactant's mixing-cup concentration of the reactant species
$const$ = integration constant
D = bulk fluid diffusivity
Da^{II} = (second) Damköhler number
Da^* = rescaled Damköhler number
$erf(x)$ = error function
$erfc(x)$ = complementary error function
j = shape parameter: = 0 for parallel plates; = 1 for circular channel
$J_\alpha(x)$ = Bessel function of order α
k = intrinsic kinetic constant (with the reaction rate expressed per volume of washcoat)
k_{surf} = intrinsic kinetic constant (with the reaction rate expressed per interface area)
L = length of the channel
LHS = left hand side
m = order of reaction in power-law kinetics
$M(a,b,z)$ = confluent (Kummer's) hypergeometric function
Pe_m = transverse Péclet number
Pe_{ax} = axial Péclet number
r = dimensionless transverse coordinate (circular channel geometry)
RHS = right hand side
s = Laplace parameter
$u(r)$ = velocity profile inside the channel
$\langle u \rangle$ = average velocity inside the channel
$u_n(R,z)$ = concentration profile relative to inlet conditions ($= c_n(R, z) - c_n(R, 0)$)
u_{max} = maximum velocity inside the channel
$v(r)$ = dimensionless velocity profile, normalized by average velocity
x = dimensionless transverse coordinate (parallel plates geometry)
X_R = conversion of reactant
w_n = nth Fourier weight
z = dimensionless axial coordinate

Greek letters

α = aspect ratio of the channel
δ = thickness of the concentration boundary layer; gauge function of the perturbation parameter
ε = perturbation parameter
γ = axial position dependent function in concentration profile
$\Gamma(x)$ = gamma function, $\int_0^\infty t^{x-1}e^{-t}dt$
η = catalytic coating effectiveness factor
φ_n = nth eigenfunction
λ_n = nth eigenvalues
σ = shape/flow parameter, $(j+1)u_{max}/\langle u \rangle$
τ = time constant

Superscript

$\hat{}$ = dimensional quantity
$\bar{}$ = Laplace transform with respect to z

Subscript

∞ = in the Dirichlet limit
max = maximum
n = order in perturbation problem

Literature Cited

1. Van de Ven J, Rutten GMJ, Raaijmakers MJ, Giling LJ. Gas phase depletion and flow dynamics in horizontal MOCVD reactors. *J Crys Growth*. 1986;76:352–372.
2. Newman JS. *Electrochemical Systems*, 1st ed. Englewood Cliffs, N.J.: Prentice-Hall, Inc., 1973.
3. Bhattacharya M, Harold MP, Balakotaiah V. Shape normalization for catalytic monoliths. *Chem Eng Sci*. 2004;59:3737–3766.
4. Tronconi E, Forzatti P. Adequacy of lumped parameter models for SCR reactors with monolith structure. *AIChE J*. 1992;38:201–210.
5. Berger RJ, Kapteijn F. Coated-wall reactor modeling-criteria for neglecting radial concentration gradients. 1. Empty reactor tubes. *Ind Eng Chem Res*. 2007;46:3863–3870.
6. Kockmann N. *Transport Phenomena in Micro Process Engineering*, 1st ed. Berlin: Springer-Verlag, 2008.
7. Gervais T, Jensen KF. Mass transport and surface reactions in microfluidic systems. *Chem Eng Sci*. 2006;61:1102–1121.
8. Hessel V, Hardt S, Löwe H. *Chemical Micro Process Engineering: Fundamentals, Modelling and Reactions*. Weinheim: Wiley-VCH, 2004.
9. Graetz L. Ueber die Wärmeleitungsfähigkeit von Flüssigkeiten. *An Phys Chemie*. 1883;18:79–94.
10. Paneth F, Herzfeld KF. Free methyl and free ethyl. *Z Elektrochem Angew Phys Chem*. 1931;37:377–582.
11. Nusselt W. Die Abhängigkeit der Wärmeübergangszahl von der Rohrlänge. *Zeitschrift des Vereines deutscher Ingenieure*. 1910;54:1154–1158.
12. Damköhler G. Einfluss von Diffusion, Strömung, und Wärmetransport auf die Ausbeute in Chemisch-Technischen Reaktionen. *Chem Eng Tech*. 1937;3:359–485.
13. Carslaw HS, Jaeger JC. *Conduction of Heat in Solids*, 2nd ed. New York: Oxford University Press, 1959.
14. Bauer HF. Diffusion, convection and chemical reaction in a channel. *Int J Heat Mass Transfer*. 1976;19:479–486.
15. Shah RK, London AL. *Laminar Flow Forced Convection in Ducts*. New York: Academic Press, 1978.

16. Özisik MN, Sadeghipour MS. Analytic solution for the eigenvalues and coefficients of the graetz problem with third kind boundary condition. *Int J Heat and Mass Transfer*. 1982;25:736–739.
17. Sellars J, Tribus M, Klein J. Heat transfer to laminar flow in a round tube or flat conduit—the Graetz problem extended. *ASME Trans* 1956;78:441–448.
18. Brown GM. Heat or mass transfer in a fluid in laminar flow in a circular or flat conduit. *AIChE J*. 1960;6:179–183.
19. Solbrig CW, Gidaspow D. Convective diffusion in a parallel plate duct with one catalytic wall-laminar flow—first order reaction. *Can J Chem Eng* 1967;45:35–39.
20. Newman J. *The Graetz problem*. In: A. J. Bard (ed.), *The Fundamental Principles of Current Distribution and Mass Transport in Electrochemical Cells*. New York: Dekker, 1973:187–352.
21. Kays WM, Crawford ME. *Convective Heat and Mass Transfer*, 2nd ed. New York: McGraw-Hill, 1980.
22. Housiadas C, Larrodbeé FE, Drossinos Y. Numerical evaluation of the Graetz series. *Int J Heat Mass Transfer*. 1999;42:3013–3017.
23. Balakotaiah V, West DH. Shape normalization and analysis of the mass transfer controlled regime in catalytic monoliths. *Chem Eng Sci*. 2002;57:1269–1286.
24. Bhattacharya M, Harold MP, Balakotaiah V. Mass-transfer coefficients in washcoated monoliths. *AIChE J*. 2004;50:2939–2955.
25. Petersen E. *Chemical Reaction Analysis*, 1st ed. New Jersey: Prentice-Hall Inc., 1965.
26. Pancharatnam S, Homsy GM. An asymptotic solution for tubular flow reactor with catalytic wall at high Peclet numbers. *Chem Eng Sci*. 1972;27:1337–1340.
27. Ghez R. Mass transport and surface reactions in Lévêque's approximation. *Int J Heat Mass Transfer*. 1978;21:745–750.
28. Worsøe-Schmidt PM. Heat transfer in the thermal entrance region of circular tubes and annular passages with fully developed laminar flow. *Int J Heat and Mass Transfer*. 1967;10:541–551.
29. Newman Newman J. Extension of the Leveque solution. *J Heat Transfer*. 1969;91:177–178.
30. Gottifredi JC, Flores AF. Extended Leveque solution for heat transfer to non-Newtonian fluids in pipes and flat ducts. *Int J Heat and Mass Transfer*. 1985;28:903–908.
31. Shih YP, Huang CC, Tsay SY. Extended Leveque solution for laminar heat transfer to power-law fluids in pipes with wall slip. *Int J Heat and Mass Transfer*. 1995;38:403–408.
32. Acrivos A, Chambré PL. Laminar boundary layer flows with surface reactions. *Industrial & Engineering Chemistry*. 1957;49:1025–1029.
33. Siegel R, Sparrow EM, Hallman TM. Steady laminar heat transfer in a circular tube with prescribed wall heat flux. *Appl Sci Res*. 1958;7:386–392.
34. Compton RG, Unwin PR. The Dissolution of Calcite in Aqueous Solution at pH < 4: Kinetics and Mechanism. Philosophical Transactions of the Royal Society of London. *Series A, Mathematical and Physical Sciences*. 1990;330:1–45.
35. Rosner DE. Effects of convective diffusion on the apparent kinetics of zeroth order surface-catalysed chemical reactions. *Chem Eng Sci*. 1966;21:223–239.
36. Chambré PL, Acrivos A. On chemical surface reactions in laminar boundary layer flows. *J Appl Phys*. 1956;27:1322–1328.
37. Katz S. Chemical reactions catalysed on a tube wall. *Chem Eng Sci*. 1959;10:202–211.
38. Rosner DE. The apparent chemical kinetics of surface reactions in external flowsystems: Diffusional falsification of activation energy and reaction order. *AIChE J*. 1963;9:321–331.
39. Grau RJ, Cabrera MI, Cassano AE. The laminar flow tubular reactor with homogeneous and heterogeneous reactions. I. Integral Equations for Diverse Reaction Rate Regimes. *Chem Eng Commun*. 2001;184:229–257.
40. Lopes JP, Cardoso SSS, Rodrigues AE. Multiscale perturbation analysis of mass transfer and reaction in a microchannel with porous catalytic coating. AIChE Annual meeting, Nashville, TN, 2009.
41. Lévêque MA. Les lois de la transmission de chaleur par convection. *Ann Mines*. 1928;13:201–299.
42. Bird RB, Stewart WE, Lightfoot EN. *Transport Phenomena*. 1960. New York: Wiley.
43. Deen WM. *Analysis of Transport Phenomena*, 1st ed. New York: Oxford University Press, 1998.
44. Keyser LF, Moore SB, Leu MT. Surface reaction and pore diffusion in flow-tube reactors. *J Phys Chem* 1991;95:5496–5502.
45. Hayes RE, Liu B, Moxom R, Votsmeier M. The effect of washcoat geometry on mass transfer in monolith reactors. *Chem Eng Sci*. 2004;59:3169–3181.
46. Townsend JS. The diffusion of ions into gases. *Philos Trans R Soc London Ser A*. 1900;193:129–158.
47. Rice RG, Do DD. *Applied Mathematics and Modeling for Chemical Engineers*. New York: John Wiley & Sons, 1995.
48. Schmidt LD. *The Engineering of Chemical Reactions*. New York: Oxford University Press, 1998.
49. Belfiore LA. *Transport Phenomena for Chemical Reactor Design*. Hoboken, NJ: John Wiley & Sons, Inc., 2003.
50. Abramowitz M, Stegun IA. *Handbook of Mathematical Functions*. 1972. Washington, DC: National Bureau of Standards.
51. Gottifredi JC, Gonzo EE. *Application of perturbation and matching techniques to solve transport phenomena problems*. In: A. S. Mujumdar and R. A. Mashelkar (eds.), *Advances in Transport Processes*. New Delhi: Wiley Eastern, 1986:419–464.
52. Villermaux J. Diffusion in a cylindrical reactor. [Diffusion dans un reacteur cylindrique]. *Int J Heat and Mass Transfer*. 1971;14:1963–1981.
53. Houzelot JL, Villermaux J. Mass transfer in annular cylindrical reactors in laminar flow. *Chem Eng Sci*. 1977;32:1465–1470.
54. Haji-Sheikh A, Beck JV, Amos DE. Axial heat conduction effects in the entrance region of circular ducts. *Heat Mass Transfer*. 2009;45:331–341.
55. Churchill SW, Usagi R. A standardized procedure for the production of correlations in the form of a common empirical equation. *Ind Eng Chem*. 1974;13:39–44.
56. Groppi G, Tronconi E. Theoretical analysis of mass and heat transfer in monolith catalysts with triangular channels. *Chem Eng Sci*. 1997;52:3521–3526.
57. Cowherd Jr C, Hoelscher HE. Kinetics of fast interfacial reactions in laminar tube flow. *Ind Eng Chem Fundam*. 1965;4:150–154.
58. Levich VG. *Physicochemical Hydrodynamics*. Englewood Cliffs, N.J.: Prentice-Hall, 1962.
59. Lighthill MJ. Contributions to the theory of heat transfer through a laminar boundary layer. *Proc R Soc London Ser A*. 1950;202:395–377.
60. Colle S. The extended Graetz problem with arbitrary boundary conditions in an axially heat conducting tube. *Appl Sci Res*. 1988;45:33–51.

Appendix A: Structure of the Perturbation Problem in Lévêque's Regime

In the presence of significant consumption of reactant (with an associated concentration drop, $\Delta c \sim O(1)$), transverse (and axial) gradients are much larger than $O(1)$ and we stretch independent variables to obtain a correct rescaling:

$$\frac{\partial^2 c}{\partial X^2} + \alpha^2 \delta_X^2 \frac{\partial^2 c}{\partial z^2} = \alpha Pe_m v(X) \delta_x^2 \frac{\partial c}{\partial z} \quad \text{for parallel plates} \quad \text{(A1a)}$$

$$\frac{\partial^2 c}{\partial R^2} - \frac{\delta_R}{1-\delta_R}\frac{\partial c}{\partial R} + \alpha^2 \delta_R^2 \frac{\partial^2 c}{\partial z^2} = \alpha Pe_m \delta_R^2 v(R) \frac{\partial c}{\partial z} \quad \text{for a circular channel.} \quad \text{(A1b)}$$

The velocity profiles given by Eq. (2) become

$$v(X) = \begin{cases} 3\delta_x X\left(1 - \frac{\delta_X X}{2}\right) & \text{laminar flow} \\ 1 & \text{plug-flow} \end{cases} \text{ and}$$

$$v(R) = \begin{cases} 4\delta_R R\left(1 - \frac{\delta_R R}{2}\right) & \text{laminar flow} \\ 1 & \text{plug-flow} \end{cases}$$

where $R = (1 - r)/\delta_R$ and $X = (1 - x)/\delta_X$ are the transverse stretched spatial variables, and δ_X, $\delta_R \ll 1$ are the dimensionless thicknesses of the concentration boundary layer near the

wall. The distinguished limit in Eqs. (A1) reflects a convection - transverse diffusion dominance. Balancing those two terms, the inner layer scales become: $\delta_R \sim \delta_X \sim (\alpha Pe_m)^{-1/2}$ for plug flow and $\delta_X \sim (3\ \alpha\ Pe_m)^{-1/3}$ for laminar flow between parallel plates or $\delta_R \sim (4\alpha\ Pe_m)^{-1/3}$ if a parabolic velocity profile inside a circular channel is considered. We kept the axial diffusion term in Eqs. (A1) but near the wall its importance relative to transverse diffusion is $O(Pe_{ax}^{-1})$ for plug-flows, while for laminar flows its effect only shows up at $O(\alpha^{2/3}/Pe_{ax}^{2/3})$, which are smaller than any other terms calculated next.

We can see the convection-dominated limit as a perturbation problem, where Lévêque's solution is nothing but the leading-order result. The inner problem given by Eqs. (A1) can be decomposed into subproblems once the dependent variable in this region is expanded as a series in $\boldsymbol{\delta}$, i.e., at the boundary layer ($c^{bl} \equiv c$):

$$c(R, z; \alpha Pe_m) = \sum_{n=0}^{\infty} c_n(R, z)\delta^n \tag{A2}$$

Since the flux continuity at the interface is explicitly free of the perturbation parameter, the appropriate rescaled form for the $O(\delta^n)$ subproblem is (replace R by X for parallel plates)

$$\left.\frac{\partial c_n}{\partial R}\right|_{R=0} = Da^* c_n(R = 0, z) \tag{A3}$$

Here however, Da^* ($=Da^{II}\ \eta\ \delta_R$) includes the correct length scale for the concentration gradient ($a\ \delta_R$). For $Da^* \sim 1$, Eq. (A3) must retain its full structure, but Neumann and Dirichlet conditions are natural limits for $Da^* \ll 1$ and $Da^* \gg 1$.

The inlet boundary condition is homogeneous ($c_n\ (R,\ 0) = 0$) for $n \geq 1$ and the general matching procedure can be reduced in this case to Prandtl's condition for $n = 0$:

$$c_0(R \to \infty, z) \to c^{out}(r, z) = 1(\text{finite}),\ \text{and} \tag{A4a}$$

$$c_n(R \to \infty, z) = 0 \qquad \text{for } n \geq 1. \tag{A4b}$$

Then, the composite solution is simply given by

$$c(r, z) = c^{out}(r, z) + c^{bl}(R, z) - cp$$

where $cp = \lim_{R\to\infty} c_0^{bl}(R, z) = c^{out}(r, z)$, and therefore the solution in the boundary layer is uniformly valid over the complete transverse domain.

At leading order, the simplified form of the inner equations in the variables X or R becomes independent of the geometry (curvature effects are of $O(\delta_R)$ and therefore neglected). Moreover, the laminar parabolic velocity profile is linear up to $O(\delta_R)$ near the wall (Figure 1). This reproduces Lévêque's analysis[42] and assumptions.

Appendix B: Higher Order Corrections to Lévêque's Problem

The higher order problem accounting for curvature can be extracted from Eqs. (A1) (plug-flow profile) at $O[(\alpha\ Pe_m)^{-1/2}]$ and is given by

$$\frac{\partial^2 c_1}{\partial R^2} - \frac{\partial c_1}{\partial z} = \frac{\partial c_0}{\partial R} \tag{B1}$$

with boundary conditions given for $n = 1$ in Eqs. (A3). The surface concentration value is calculated inverting the Laplace transform

$$\overline{c}_1(R = 0, s) = -\frac{Da^*}{2(Da^* + \sqrt{s})^2 s}.$$

The correction accounting for nonlinearity in the velocity profile at the boundary layer appears at $O(\delta) \sim O[(\alpha\ Pe_m)^{-1/3}]$ and is calculated from

$$\frac{\partial^2 c_1}{\partial X^2} - X\frac{\partial c_1}{\partial z} = -\frac{X^2}{2}\frac{\partial c_0}{\partial z}$$
$$\text{at } O[(3\alpha Pe_m)^{-1/3}] \text{ for parallel plates, and} \tag{B2a}$$

$$\frac{\partial^2 c_1}{\partial R^2} - R\frac{\partial c_1}{\partial z} = -\frac{R^2}{2}\frac{\partial c_0}{\partial z} + \frac{\partial c_0}{\partial R}$$
$$\text{at } O[(4\alpha Pe_m)^{-1/3}] \text{ for a circular channel.} \tag{B2b}$$

Solving Eqs. B2 with Laplace transform and then inverting in the limits of high and low Da^* yields Eqs. 33–34.

Appendix C: Langmuir Kinetics in Developing Concentration Profile Conditions

Langmuir-type kinetics only dependent on the local concentration of one reactant next to the surface can also be considered (although it is known that for some parameter combinations multiplicity behavior may show up):

$$\mathcal{R}\{c(R = 0, z)\} = \frac{k_{surf}\ c^p(0, z)}{[1 + Kc(0, z)]^q},$$

where K, p and q are kinetic parameters. With more or less complexity, this case can also be dealt by the same procedure. We restrict ourselves to the equivalence with the "power law" kinetic model in the $Da^* \ll 1$ and $\gg 1$ limits without considering any multiplicity phenomena. In this case, the wall boundary condition is

$$\left.\frac{\partial c}{\partial R}\right|_{R=0} = Da^*(1 + K)^q \left.\frac{c^p}{(1 + Kc)^q}\right|_{R=0}, \tag{C1}$$

where p, q and K are the additional kinetic parameters, and $Da^* = \frac{a}{D}\frac{\mathcal{R}\{\hat{c}\}_{in}}{\hat{c}_{in}}$ with $\mathcal{R}\{\hat{c}_{in}\} = k_s \hat{c}_{in}^p/(1 + K)^q$. The rate expression in Eq. C1 can be thought as a generalized unimolecular decomposition kinetics, reducible to power-law reaction rate when $p = m$ and q or K equals zero.

Under kinetic control, concentration deviates little from the inlet concentration, and a correction to that solution respects the following boundary condition:

$$\left.\frac{\partial c_1}{\partial R}\right|_{R=0} = (1 + K)^q \frac{c_0^p(0, z)}{(1 + Kc_0^q(0, z))^q} = 1, \tag{C2}$$

which is identical to Eq. 45. Also at the next order $O(Da^*)^2$, the results are the same as the ones in Eqs. 48 as long as m is redefined as

$$m = p - \frac{qK}{1+K}, \tag{C3}$$

since at this order the boundary condition is written as

$$\left.\frac{\partial c_2}{\partial R}\right|_{R=0} = \left(p - \frac{qK}{1+K}\right) c_1(0,z). \tag{C4}$$

For external mass transfer control conditions (ε=1/Da*), the $O(\delta_1)$ correction to Dirichlet's limit (Eqs. 52) obeys at the wall,

$$\frac{\varepsilon}{(1+K)^q}\left.\frac{\partial c_0}{\partial R}\right|_{R=0} = \frac{(c_1(0,z)\delta_1)^p}{(1+Kc_1(0,z)\delta_1)^q} \sim (c_1(0,z)\delta_1)^p. \tag{C5}$$

Since $\delta_1 \ll 1$, the balance in Eq. C5 reduces the problem again to "power law" wall kinetics type ($K\ \delta_1 \ll 1$). In this case, $p = m$ in Eq. 50 and $\delta_1 \sim \varepsilon^{1/p}/(1+K)^{q/p}$.

Manuscript received Aug. 9, 2010, and revision received Oct. 13, 2010.